NASA-CR-176403
19860003832

A Reproduced Copy

OF

N86-13300

Reproduced for NASA

by the

NASA Scientific and Technical Information Facility

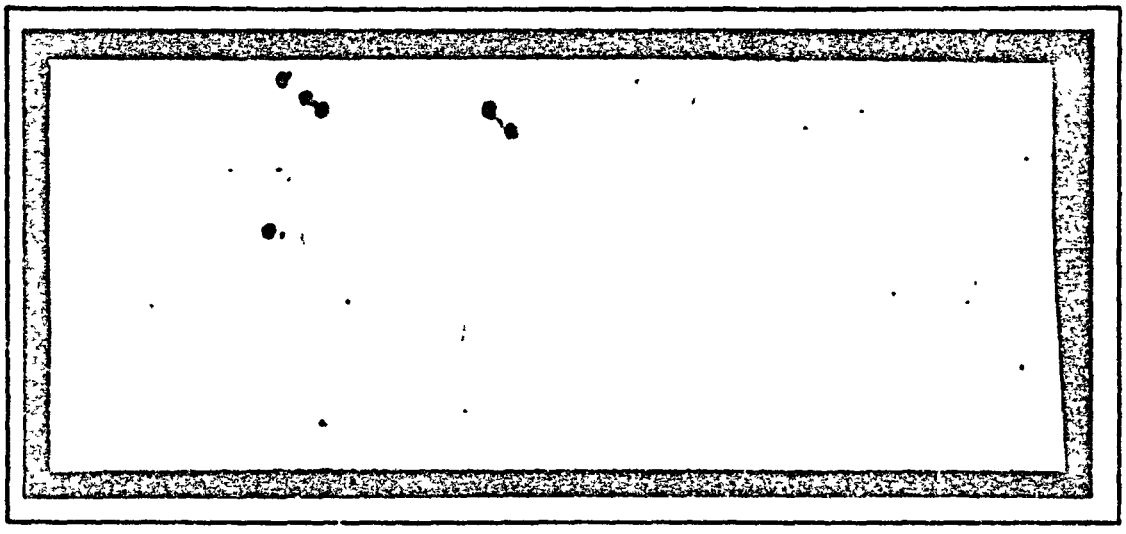

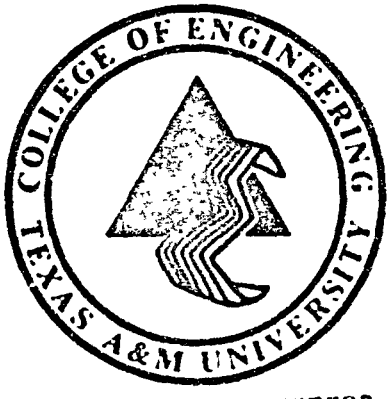

College of Engineering
Texas A&M University

A DIRECT-INVERSE METHOD FOR TRANSONIC AND SEPARATED FLOWS ABOUT AIRFOILS

TAMRF Report No. 3224-85-12

December 1985

Final Report
NASA Grant NSG-1174

Leland A. Carlson
Professor
Aerospace Engineering Department
Texas A&M University
College Station, TX 77843-3141

A DIRECT-INVERSE METHOD FOR TRANSONIC AND SEPARATED FLOWS ABOUT AIRFOILS

Leland A. Carlson

Aerospace Engineering Department

Texas A&M University

SUMMARY

A direct-inverse technique and computer program called TAMSEP that can be used for the analysis of the flow about airfoils at subsonic and low transonic freestream velocities is presented. The method is based upon a direct-inverse nonconservative full potential inviscid method, a Thwaites laminar boundary layer technique, and the Barnwell turbulent momentum integral scheme; and it is formulated using Cartesian coordinates. Since the method utilizes inverse boundary conditions in regions of separated flow, it is suitable for predicting the flowfield about airfoils having trailing edge separated flow under high lift conditions. Comparisons with experimental data indicate that the method should be a useful tool for applied aerodynamic analyses.

SYMBOLS

a	isentropic speed of sound
c_3^*	boundary layer coefficient in separated pressure correlation
C_p	pressure coefficient
M	Mach number
q	velocity
U,V	velocity component in the x or y direction respectively
U_e	transformed velocity at boundary layer edge
u	velocity in the boundary layer
u^*, u_ℓ	law-of-the-wall and law-of-the-wake velocity parameters
x,y	Cartesian coordinates
α	angle of attack
γ	ratio of specific heats, assumed to be 1.4
Γ	circulation
δ	boundary layer thickness
θ	polar coordinate
ξ, η	computational coordinates
Φ	potential function
φ	perturbation potential

SYMBOLS (Continued)

Subscripts:

∞	freestream condition
b	body
e	boundary layer edge
i,j	grid location
LE	leading edge
TE	trailing edge
ξ,η,x,y	differentiation

GENERAL DESCRIPTION

INTRODUCTION

Over the past decade, several finite-difference potential flow methods[1-3] have been developed and successfully used for the design and analysis of subsonic and transonic airfoils at and near cruise conditions. However, in the analysis of high performance airfoils, aerodynamicists would also like to be able to predict airfoil pressure distributions and aerodynamic coefficients at high lift, high angle-of-attack conditions. Since such situations are frequently characterized by regions of separated flow on the upper surface and are dominated by strong viscous interaction effects, inviscid methods alone are not applicable. Furthermore, subsonic-transonic analysis methods[3,4] which couple inviscid and boundary layer solutions typically only include the effects of weak viscous interaction and generally fail to give accurate results when separated flow exists on the upper surface.

However, it has been demonstrated[5-8] that the direct-inverse technique coupled to a suitable boundary layer method can be successfully applied to low speed flows about airfoils having massive separation. In addition, Barnwell[9], Dvorak and Choi[10], and Taverna[11] have developed similar methods for transonic flows. Barnwell's method, however, is limited in application in that it utilizes for its inviscid solver the transonic small perturbation equation. Further, References 9 and 11 only include the effects of viscous interaction due to a turbulent boundary layer. On most airfoils, particularly on the lower surface at high angles of attack, extensive regions of laminar flow exist.

This report describes a flow model and computer program, called TAHSEP, which can be used to predict the flowfield about a single element transonic airfoil at high angle of attack high lift conditions with trailing edge separation. Since the method is based upon the TRANDES[4] and TRANSEP[6] codes, it can also be used for subsonic-transonic analyses not involving separation.

METHOD OF APPROACH

The present approach is based upon the direct-inverse method developed in the TRANDES and TRANSEP programs and the ability of this method to use either the displacement surface (airfoil ordinate plus displacement thickness) or pressure as the airfoil boundary condition. For the high angle-of-attack case, the airfoil lower surface only experiences weak viscous interaction and frequently has a long laminar run before transitioning to fully turbulent flow. Thus, the present model includes an initial laminar boundary layer calculation in its viscous interction section. On the upper surface the boundary layer is also intially laminar, but it quickly becomes turbulent in character followed in many cases by boundary layer separation and a separated zone which can extend over a significant portion of the airfoil surface. In the present model, this separated region is treated inversely in that the pressure distribution along the effective displacment surface streamline is determined iteratively as part of the solution and used as the airfoil boundary condition. Consequently, the present method has been modeled as shown on Figure 1.

To obtain the inviscid portion of the flowfield, the full potential equation for two-dimensional compressible flow is used in nonconservative form as

$$(a^2 - \bar{\Phi}_x^2)\bar{\Phi}_{xx} - 2\bar{\Phi}_x\bar{\Phi}_y\bar{\Phi}_{xy} + (a^2 - \bar{\Phi}_y^2)\bar{\Phi}_{yy} = 0 \qquad (1)$$

where the subscripts denote partial differentiation. By defining a perturbation potential, ϕ, such that

$$\Phi = x q_\infty \cos\alpha + y q_\infty \sin\alpha + q_\infty \phi \tag{2}$$

where the velocity components are given by

$$\begin{aligned} U &= \Phi_x = q_\infty(\cos\alpha + \phi_x) \\ V &= \Phi_y = q_\infty(\sin\alpha + \phi_y) \end{aligned} \tag{3}$$

the governing equation in terms of the perturbation potential can be written as

$$(a^2 - U^2)\phi_{xx} - 2UV\phi_{xy} + (a^2 - V^2)\phi_{yy} = 0 \tag{4}$$

with

$$a^2 = a_\infty^2 - \left(\frac{\gamma-1}{2}\right)(U^2 + V^2 - q_\infty^2) \tag{5}$$

The nonconservative form of the potential equation was selected for the present problem because for two-dimensional flows results obtained with it agree better with Euler solutions than those obtained using the fully conservative form of the equation.[12] In addition, the conservative formulation appears to break down in two-dimensional cases shortly after the onset of supercritical flow.[13]

In the present model, Equations (3-5) are finite differenced using a rotated difference scheme and solved iteratively using column relaxation in a stretched Cartesian grid which maps the infinite domain to a finite computational box. The appropriate boundary condition at infinity is

$$\phi = -\frac{\Gamma}{2\pi} \tan^{-1}\left(\sqrt{1-m_\infty^2}\,(\theta-\alpha)\right) \tag{6}$$

where θ is the polar angle, and Γ is the circulation, which is determined by the change in potential across the Kutta-Joukowski cut at the trailing edge of the airfoil.

Likewise, the appropriate airfoil boundary condition in the direct regions (regions without separation having only weak viscous interaction) is the flow tangency condition given by the ordinates of the airfoil displacement surface, i.e.

$$\left(\frac{dy}{dx}\right)_b = \left(\frac{V}{U}\right)_b = \frac{q_\infty\,(\sin\alpha + \phi_{y_b})}{q_\infty\,(\cos\alpha + \phi_{x_b})} \tag{7}$$

In the inverse or separated flow region the pressure distribution along the effective displacement surface streamline is considered specified and used as the boundary condition. As shown in Reference 2, this approach leads to a derivative boundary condition for the inverse region of the form

$$(\phi_x)_b = -\cos\alpha + \left\{\frac{1}{1+\left(\frac{v}{U}\right)_b}\left\{1-\left\{\left[1+\frac{\gamma m_\infty^2 C_{p_b}}{2}\right]^{\frac{\gamma-1}{\gamma}}-1\right\}\frac{2}{(\gamma-1)m_\infty^2}\right\}\right\}^{1/2} \tag{8}$$

Complete details concerning the finite difference scheme, the stretched Cartesian grid system, and the treatment of the boundary conditions are given in References 1,2, and 4.

To include viscous effects, the basic approach is to calculate a boundary layer displacement thickness for the weak interaction regions and to use it to correct the location of the displacement surface (i.e., airfoil ordinate plus displacement thickness). For the strongly interacting separated zone on the upper surface, the pressure is determined from the interaction solution and the location of the displacement surface is computed by integrating the surface tangency condition, Eq. (7), with the initial conditions specified by the displacement surface ordinates at the separation point, which is the interface between the two regions. The location and slopes of the displacement surfaces are updated regularly throughout the iterative solution.

In the present method, the laminar portion of the boundary layer is computed using a compressible Thwaites method similar to that used previously in TRANSEP.[6] The transition location is determined from a Granville type correlation[14] based upon the difference between the local momentum thickness Reynolds number and the value at the laminar instability point combined with the pressure gradient history. Sometimes, particularly on the upper surface at high angles of attack, laminar separation is predicted upstream of the transition point. In these cases, the local momentum thickness Reynolds number is compared to an empirical correlation in order to determine if the laminar bubble is long or short. If the bubble is short, its length is assumed to be one horizontal delta-x grid width and the turbulent flow computation is initiated at the next downstream grid point. If the estimate indicates that the bubble is long, the calculation proceeds, but a warning is printed which indicates that the results are probably in error.

After transition, the turbulent boundary layer is computed using the simplified Kuhn and Nielsen method (SKAN) as developed by Barnwell in Reference 9. This method was selected because it is efficient, reliable, and yields excellent predictions of displacement thicknesses and separation point location. The SKAN turbulent boundary layer method solves the integral forms of the momentum equation, moment of momentum equation, and the derivative of the Coles' law-of-the-wall law-of-the wake relationship applied at the boundary layer edge. After considerable effort[9], these equations can be transformed into a set of simultaneous ordinary differential equations, i.e.

$$a_{i1}\frac{du^*}{dx} + a_{i2}\frac{du_p}{dx} + a_{i3}\frac{d\delta}{dx} = b_i\frac{dV_e}{du_e}\frac{du_e}{dx} + \frac{a_0}{a_\infty}c_i \qquad i = 1,2,3 \qquad (9)$$

which can be solved for the wall friction velocity, u^*, the wake parameter u_p, and the boundary layer thickness δ, using a second-order predictor-corrector technique. The remaining quantities of interest such as displacment thickness and momentum thickness are then determined from these variables. The numerical integration is terminated at the separation point, where the wall friction velocity, u^*, vanishes.

The method uses a two-layer eddy-viscosity model, which ignores the viscous sublayer terms, consisting of an inner layer Prandtl mixing length model and an outer layer Clauser model; and the intermittency factor as well as several density ratios appearing in the fundamental equations are approximated. In addition, the method assumes an adiabatic wall.

Thus, on the lower surface the flow is computed using direct boundary conditions (airfoil specified) including the effects of weak viscous interaction. On the upper surface, the flowfield is also computed directly with viscous interaction up to the separation point, which is determined as part of the boundary layer solution. Downstream of separation, inverse boundary conditions are utilized, and the pressure must be specified. Fortunately, if the skin friction at the wall is assumed to be zero in the separated zone, the SKAN formulation can be used to obtain a closed form solution for the velocity, and hence the pressure, at the outer edge of the separated zone. The resultant analytic expressions for the velocity and pressure are

$$\frac{u_e}{V_\infty} = \frac{5}{6}\,\frac{c_3^*\left(\cos\alpha\,(x_{TE}-x_{sep})+\phi_{TE}-\phi_{sep}\right)}{\left\{\left[1+c_3^*(x_{TE}-x_{sep})\right]^{6/5}-1\right\}\left[1+c_3^*(x-x_{sep})\right]^{1/2}} \tag{10}$$

$$C_p = \frac{2}{\gamma M_\infty^2}\left(\left(1+\frac{\gamma-1}{2}M_\infty^2\left(1-\frac{u_e^2}{V_\infty^2}\right)\right)^{\frac{\gamma}{\gamma-1}}-1\right) \tag{11}$$

As can be seen, the separated pressure depends upon the flowfield solution via the inviscid perturbation potentials at the separation point and the trailing edge, the size of the separated zone, and thru c_3^* the boundary layer solution at the separation point. In addition, this closed form solution predicts a variable pressure distribution for the separated region. At low freestream Mach numbers this variation is extremely small and is essentially constant. However, at freestream Mach numbers of 0.3 and above, the variation becomes signficant and influences the resultant flowfield solution. This trend and separated pressure variation is in accord with experimental observations and is a significant improvement over previous methods which assumed constant pressure in the separated zone regardless of flow conditions. However, since at low speeds the

separated pressure is essentially constant and the complexity introduced by Equations (10-11) may not be warranted, the present method contains the option of either using a constant pressure in the separated region or the variable distribution determined by the closed form solution given above.

In principle, the separated region and the wake should be accurately modeled with respect to physical phenomena and internal details, and this approach has been taken by other investigators[10,15-16]. In the present model, however, the wake region contains very few computational points since the coordinate system rapidly stretches to infinity. Thus, the wake is assumed to be inviscid with a constant pressure trailing edge formed by the upper and lower displacement surfaces. Fortunately, extensive numerical experiments with the present and previous[7] models indicate that the pressure distribution and aerodynamic coefficients are primarily dependent upon obtaining accurate predictions for the location of the separation point and the magnitude and variation of the separated pressure. Apparently, the details of the wake region are of secondary importance. Since the present method obtains the separation point location directly from the solution for the wall friction velocity, u^*, and the pressure variation from a solution which couples the inviscid and viscous parts, it should yield reasonable engineering results.

INTERACTION AND ITERATION PROCEDURE

The iteration and interaction procedure used in TAMSEP is similar to that used in the low-speed program TRANSEP[6], and it is outlined in schematic form on Figure 2. The program first reads all necessary input and initializes the perturbation potential at all grid points to zero. Next it computes

transformation factors and coordinates associated with the stretched Cartesian grid for the initial grid specified by the input data. Included in this process is the computation of all airfoil ordinates and slopes required on the computational grid.

Since the initial grid is normally very coarse with a default size of 13 x 7, only fifty inviscid iterative cycles are computed on this grid. The calculation procedure used for the inviscid potential equation is the same iterative successive column over-relaxation scheme used in TRANDES1,[4]. This limited number of cycles serves to rapidly create an approximate starting solution for succeeding grids. After these are completed, the grid is then halved and the solution interpolated onto a new grid, which has a default size of 25 x 13.

After obtaining all necessary coordinates, stretching factors, airfoil ordinates and slopes, etc., for this second grid, the method then performs fifty inviscid iterative cycles before considering any type of viscous interaction. Experience has shown that it is important to perform a limited number of inviscid cycles at the beginning of each new grid in order to eliminate any "problems" introduced by grid halving and interpolation.

After these initial iterations, the program then checks to see whether or not the user desires viscous interaction to be included by examining the value of the variable ITACT. If viscous interaction is desired, which is specified by the ITACT default value of one, the program then checks to see if an initial laminar boundary layer is to be included (ILAM=1) or if the viscous calculations are to be for a turbulent boundary layer with user specified transition points (ILAM=0).

Upon completing the boundary layer computations for the current flowfield solution, the program then calculates the ordinates and slopes of the upper and lower displacement surfaces. Since it only involves weak viscous interaction, the lower surface computations are from the leading edge or the lower surface stagnation point, whichever is further aft, to the trailing edge. However, on the upper surface they are only from the leading edge to the separation point or to the trailing edge, whichever is less. This process involves smoothing of the displacement thickness values, properly adding them to the airfoil ordinates, and spline fitting the resulting points.

At this point the procedure depends upon whether or not separation has been detected on the upper surface. If separation does not exist prior to the last grid point on the airfoil upper surface, additional inviscid cycles are performed before returning to the viscous interaction loop. However, if separation is predicted, then the method must determine the pressure distribution and the location of the displacement surface in the separated zone.

Exactly how the separated pressure distribution is determined depends upon the user specified variable KSEP. If KSEP is zero, the pressure is assumed to be constant in the separated zone and is computed by

$$C_{p_{sep}} = \frac{-2(\varphi_{TE} - \varphi_{sep})}{x_{TE} - x_{sep}} \tag{12}$$

While this expression is a small perturbation approximation for $C_{p,sep}$, its usage has been found to be accurate and adequate for low speed incompressible flows. At freestream Mach numbers of 0.3 and higher, however, the variable separated pressure option, specified by a KSEP value of one, should be used. In this case, the pressure distribution along the displacement streamline in the separated

region is determined by Equations (10) and (11) above. Note that both approaches determine the separated zone pressure, which depends upon the current solution, by conditions at both the separation point and at the trailing edge and not just on conditions in the vicinity of separation. This result is in agreement with the conclusion of Gross[17] that conditions at the downstream end of the separation zone partially influence the separation pressure level.

After determining the separated pressure distribution corresponding to the predicted separation point and the current potential flow solution, the corresponding upper surface displacement surface must also be computed for the separated zone. When separation exists, the previous method of adding the computed displacement thickness to the original airfoil ordinates is inappropriate since the values for displacement thickness predicted by the SKAN method are probably inaccurate in separated regions. Instead, the present approach is to solve, using the current potential flow solution, the differential equation

$$\left(\frac{dy}{dx}\right)_b = \left(\frac{V}{U}\right)_b = \frac{\sin\alpha + g_b \varphi_{x_b}}{\cos\alpha + f_b \varphi_{y_b}} \qquad (13)$$

for the y-ordinates of the separated displacement surface as a function of x. Based upon previous studies[2,6], Equation (13) is solved using the Runge-Kutta method of order four and the displacement surface ordinate at the separation point as the initial condition. In addition, in the process of solving this equation φ_{x_b} and φ_{y_b} must be evaluated by finite differences. While several formulations are possible[2], numerical studies indicate that accurate displacement surfaces are obtained using the following

$$\phi_{\eta_b} = \frac{-3\phi_{i,j-1} + 4\phi_{ij} - \phi_{i,j+1}}{2\Delta\eta} + (\eta_b - \eta_{j-1})\left(\frac{\phi_{i,j-1} - 2\phi_{ij} + \phi_{i,j+1}}{\Delta\eta^2}\right) \qquad (14a)$$

$$\phi_{s_b} = \frac{\phi_{i+1,j-1} - \phi_{i-1,j-1}}{2\Delta s} + (\eta_b - \eta_{j-1})\left(\frac{\phi_{i+1,j} - \phi_{i+1,j-1} - \phi_{i-1,j} + \phi_{i-1,j-1}}{2\Delta s\,\Delta\eta}\right) \qquad (14b)$$

In Equations (14), the point (i,j-1) is the first ghost point below the displacement surface. Its value is determined as part of the inverse prssure boundary condition.

Since the present process is iterative and the potential solution uses the separated pressure distribution as an inverse boundary condition, the solution of Eqs. (13) and (14) should yield upon convergence a separated zone displacement surface or free streamline that is compatible with the pressure distribution and potential flow solution.

At this point in the iteration-interaction procedure a check is made to see if the solution has converged or if the maximum number of iterations for a given grid size has been exceeded. If neither situation is true, ten more inviscid cycles with the new displacement surfaces and separated pressure distribution are performed prior to repeating the viscous interaction loop. If, however, either condition is satisfied and the finest grid specified by the user has not been used, the grid is refined and the entire process shown on Figure 2 is repeated. If the last grid solution has been obtained, then a final output is printed and the solution is finished.

It should be noted that the calculations on a given grid are stopped and assumed to be converged when the maximum perturbation potential change is less than some user specified value. However, when separation is present it is usual for the calculations on each grid to be terminated due to the number of iterative cycles exceeding a maximum user specified value (particularly on computers which only retain seven significant digits). In those cases, the existence or degree of convergence can be determined by examining the variation in the number of supersonic points, the location of separation, and the trailing edge ordinate of the upper displacement surface. All these values are printed out every ten iterative cycles. If they stabilize prior to the end of the computation on a given grid, then the results can be assumed to be converged. Normally, it is sufficient to perform 800 cycles on the coarse grid (25x13), 400 on the medium grid (49x25), and 400 on the fine grid ((97x49), although occasionaly more may be needed. In determining convergence, it should be remembered that the present method is supposed to obtain a steady state solution. At angles of attack above maximum lift, the actual flowfield about an airfoil is usually unsteady[17,18]. In those cases, the present method probably will not converge and may enter some type of oscillatory behavior which appears to represent an unsteady flow pattern. However, the present method is not "time-accurate" and such results should only be viewed as indicative of the presence of significant unsteady phenomena.

USER INSTRUCTIONS

CODE DESCRIPTION

The TAMSEP code consists of a main program and eighteen subroutines. The subroutines and their relationships are shown in a subroutine tree on Figure 3. The subroutine names and their functions are as follows:

FOIL -- Reads in initial airfoil shape and determines ordinates and slopes at computational points.

VISACT -- Computes turublent boundary layer when viscous interaction included.

THWAIT -- Computes the laminar boundary layer when viscous interaction included.

FIT2 -- Curve fit routine used by Thwaites method.

VALUE -- Initializes the flowfield to zero perturbation potential.

SOLVE -- Sets up the matrix coefficients used in the SLOR relaxation scheme.

PRESS -- Computes the pressure distribution on the airfoil.

COORD -- Sets up the coordinates in the computational and physical grids and computes the stretching factors.

FLOW1 -- Solves flowfield in front of the airfoil.

FLOW2 -- Solves flowfield in the direct region above and below the airfoil.

FLOW3 -- Solves flowfield in the inverse region.

WAKE -- Solves the flowfield behind the airfoil.

SHAPE -- Computes the shape of the airfoil displacement surface in the separated zone.

TRID -- Tridiagonal equation solver.

HALVE -- Doubles the grid size and interpolates old values to obtain starting values on the new grid.

PLOT -- Creates a printer plot of the C_p and displacement surface.

ARC -- Determines the arc length of the airfoil coordinates and splines the coordinates versus arc length.

SPLINE -- Computes a cubic spline thru a set of points.

The TAMSEP code is written in FORTRAN IV programming language and is designed for use on IBM, AMDAHL, CDC, DEC, and similar computers. In nonoverlay mode it requires less than 320,000 bytes on an Amdahl 470/V8. Using a FORTRAN H extended compiler at the optimization level two, it needs about 17 seconds for compilation and obtains a solution on a 97x49 grid in about 160 seconds at a rate of around 15,000 points/second. Some slight modification to formats, etc. may be required to run the program on different computer systems or under a FORTRAN 77 compiler.

INPUT DESCRIPTION

The input to the TAMSEP code is read in eight separate blocks. The first one contains a user supplied title, while the second and third blocks specify all the floating point and integer parameters needed to run the program. These parameters are input via namelists and if not specified are assigned default values by the program. Blocks four and seven are optional and are only included when the parameter IREAD is one. They read a non-zero perturbation potential starting solution and an intial airfoil description. Blocks five and eight are associated with input for the design option in the program and are only included when the parameter INV is one. Finally, block six contains the description of the airfoil under consideration. For an analysis computation, only blocks one, two, three and six would be included in the input stream.

DETAILED INPUT DESCRIPTION

Input Block 1: Title

This block consists of a single line of input and is read by the main program.

NTITLE Description of case. Up to 80 alphanumeric characters. Appears on the printed output at the beginning of the results of each grid.

Input Block 2: Floating Point Parameters

This block of input is read by the main program via a namelist called FINP.

M Freestream Mach number (real variable). Default 0.5

W Relaxation factor for subsonic points. Should be in the range 0<W<2.0. Default 1.7

X1 X location where the direct mode calculation procedure stops. In the analysis mode it should be set to 0.5 (i.e. the trailing edge). In the inverse (design) mode it is usually set to slightly less than the third point from the leading edge or larger. Default 0.5

X2 End of the inverse region. For analysis cases set to a large number. In the inverse (design) case set to 0.5 (i.e. the trailing edge). Default 10000.0

ALP Angle of attack in degrees. Default 0.0

EPS Subsonic damping factor to match difference equations at sonic line if needed. Has no effect on the accuracy of the solution. Only affects stability and convergence rate. Normally it is not needed. Default 0.0

EPSS Supersonic damping factor for iterative stability. Has no effect on the accuracy of the converged solution, only on the stability and convergence rate. Should typically be about $M^2_{max} - 1$, where M_{max} is the maximum local Mach number. Default 0.4

X4 The positive X locations where the coordinate stretching changes. It should be near the airfoil trailing edge. Default 0.49

S4 The positive psi value in the computational plane where the stretching changes. Default 2.0

CONV Convergence criteria control value. Iterations stop when the maximum change in the perturbation potential between relaxation cycles is less than CONB. Default 1.E-05

A1 Stretching constant for the Y direction. It can be used to control the Y and eta spacing near the horizontal axis. It is usually best to have the psi and eta spacing equal near the leading edge of the airfoil. Default 0.246

A2 First stretching constant for the X-direction. It is equivalent to $(2/\pi \cdot (dx/dj))$ at $\xi = j_4$. The value of A2 determines the horizontal step size near the leading and trailing edges. i.e.

$$\Delta X_{x=x4} = \frac{\pi A2}{2}\Delta\xi = \frac{\pi A2}{2}\,\frac{(2(1+S4))}{(IMAX-1)}$$

See Appendix A of Reference 4. Default 0.15

A3 Second stretching constant for the x- direction. It determines the physical location of the vertical grid line adjacent to the grid side edge. Default 3.87

RN Freestream Reynolds number based on chord length. Used only when viscous interaction (ITACT=1) included. Default 20.E+06

XIBDLY The x-location at which upper surface transition is assumed to occur. The turbulent boundary layer calculation starts at the next grid point. The relationship to percent chord is:

XIBDLY = (%chord - 50.0)/100.0

Used only if viscous interaction included (ITACT=1) and laminar boundary layer ignored (ILAM=0). Default -0.44

CIR Circulation about airfoil. If an initial solution is input (IREAD=1), it must be the corresponding value of circulation (CIR=CL/2.0). Default 0.0

CDCORR Correction to the wave drag coefficient. Because of the lack of a large number of points in the leading and trailing edge regions, the wave drag coefficient has an error associated with grid size, spacing, and lift coefficient. The magnitude of CDCORR must be determined by the user by empirical methods. Note that the correction should be different for each airfoil and grid combination. Default 0.0

RDEL Relaxation parameter for the boundary layer displcement thickness. It is used only whe viscous interaction is included (ITACT=1) and IMAX is less than or equal to 55. Default 0.25

RDELFN Fine grid relaxation parameter for the boundary layer displacement thickness. It is used only when viscous interaction is included and IMAX is greater than 55. Default 0.125

SP Maximum value allowed for the Nash-Macdonald separation parameter when x<XSEP. Used only in the design case (INV=1) when computing the boundary layer over the design surface. Default 0.004

XSEP X location after which the Nash-Macdonald separation parameter can exceed SP. Used only in the design case (INV=1) when computing the boundary layer over the design surface. Default 0.44

RCPB Not used. Ignore.

CPD Not used. Ignore.

XMON Not used. Ignore.

XLSEP Should always be initialized to 0.5. Default 0.5

XPC Location after which the lower surface displacedment thickness is required to continue decreasing once it has started to decrease. Upstream of XPC the displacement thickness is required to be monotonically increasing. For most aft-cambered airfoils it should be set to 0.1, and for conventional airfoils it should be set to 0.5. Default 0.1

XLBDLY The x-location at which lower surface transition is assumed to occur. Same relationship to chord as XIBDLY. Used only if viscous interaction included (ITACT=1) and laminar boundary layer ignored (ILAM=0). Default -0.44

RLAX Relaxation parameter for the separated pressure level in the constant separated pressure option (KSEP=0). Sometimes needed to enhance convergence. Used only when ITACT=1, IMASS=1, and KSEP=0. Default 1.0

RADIUS Leading edge radius of the airfoil nondimensionalized by the chord. Used only if ITACT=1 and ILAM=1. Default 0.0159

Input Block 2: Integer Parameters

This block of input is read by the main program via a namelist called IINP.

IMAX Number of vertical grid lines in the horizontal direction on the first grid. I=1 corresponds to upstream infinity and I=IMAX corresponds to downstream infinity. For each grid refinement IMAX is increased such that the new IMAX is two times the old value minus one. The limit on IMAX is 99. Default 13

JMAX Number of horizontal grid lines in the vertical direction on the first grid. J=1 corresponds to infinity below the airfoil and J=JMAX is infinity above the airfoil. The same formula and limit that apply to IMAX also apply to JMAX. Default 7

IKASE An integer number describing the case being computed. It is limited to a maximum of six digits and is printed at the beginning of the pressure printer plot for each grid. Default 100

INV Parameter determining the program mode. It should be zero for analysis cases and one for inverse design cases. Default 0

MITER Maximum number of interations (complete relaxation cycles) allowed on the first grid. MITER is halved for each grid refinement. However, on the fourth grid, MITER is reset to 400. Default 1600

NHALF Number of grid refinements. Default 2

ITACT Viscous interaction control parameter. It should be set to zero for analysis cases without interaction and for design cases. It should be one for analysis cases with interaction. Default 0

ISKP2 Airfoil update control parameter for grid two. It should be zero if an airfoil shape update is desired on grid two every ten iterations. It should be one it an update is not desired until grid two solution is completed. Only used in the invese design mode (INV=1). Default 0

ISKP3 Same as ISKP2 but for grid 3

ISKP4 Same as ISKP2 but for grid 4

ITERP Interpolation parameter for the design pressure distribution on grid four. If in the design mode the input pressure distribution for grid four is to be read as input data, INTERP should be zero. If it is desired to linerarly interpolate the pressure distribution of grid three, it should be one. Default 0

IREAD Starting solution control parameter. If IREAD is zero, the initial perturbation solution is assumed to be zero everywhere. If it is one, an initial solution is read as data. The latter would only normally occur when a user wished to restart a solution which had previously been saved. Default 0

LP Relaxation cycle interval at which boundary layer details are printed. For diagnostic purposes suggest 50 or 100. For normal information purposes, suggest a value of 200. Default 1000 (no printout)

IMASS Massive separation parameter. It should be one if the massive separation option is desired in analysis cases and is active only if ITACT is one. In inverse design cases (INV=1) it should be zero. Default 1

ILAM Boundary layer parameter. If zero, boundary is computed as if all turbulent with transition at XIBDLY and XLBDLY. If one, boundary layer is considered laminar-turbulent with natural transition. Default 1

IPRT1 Print parameter. If one, perturbation potential values printed at the completion of each grid. Default 0

IPRT2 Print parameter. If one, x and y velocities at each grid point printed at the completion of each grid. Default 0

KSEP Separated pressure distribution parameter. If zero, pressure in separated zone is assumed to be constant. If one, pressure in separated zone is considered variable. Default 1

Input Block 4: Starting Solution (Optional)

This block of data is read by subroutine VALUE only if the integer parameter IREAD has the value of one.

P(I,J) Nondimensional perturbation potential at point I,J. Read by rows starting at J=JMAX down to J=1. Each row runs from I=1 to I=IMAX and starts on a new line. Format 5E15.7

PB(I) Nondimensional perturbation potential at point I on the y=0 (i.e. J=JB) grid line that is associated with the lower surface of the airfoil. Read from I=1 to I=IMAX. Format 5E15.7

Input Block 5: Direct Inverse Parameters (Inverse Design Mode only)

This single line of input is read in subroutine COORD only when the inverse design mode is active (INV=1).

X1,X2 Same definition as in Block 3. However, when the inverse design mode is active, these values are read prior to the solution of each grid. This block corresponds to the first grid; and, thus, should always use X1=0.5 and X2=10000.0 Format 2F10.5

Input Block 6: Airfoil Description

This block of data is read by subroutine FOIL and describes the airfoil used in the analysis mode or the starting airfoil for the inverse design mode.

NI The number of coordinate pairs used to describe the upper surface of the airfoil. Maximum value limited to 99. Format I5

XI(I),YI(I) Coordinate pairs describing the upper surface of the airfoil. The leading edge corresponds to XI=0.0 and the trailing edge is XI=1.0. The vertical ordinate, YI, is nondimensionalized by chord. Read starting with I=1 to I=NI. Format 8F10.4

DERIX, DERIY, DERFX, DERFY Parameters describing the leading and trailing edge of the airfoil. DERIX is dx/ds of the airfoil upper surface at the leading edge. It is usually zero. DERIY is dy/ds of the airfoil upper surface at the leading edge and it is usually 1.0. DERFX is d^3x/ds^3 of the airfoil upper surface at the trailing edge. It is usually sufficiently accurate to use 0.0. DERFY is d^3y/ds^3 of the airfoil upper surface at the trailing edge. It is usually sufficiently accurate to use 0.0 . Format 4F10.4

NIB The number of coordinate pairs used to describe the lower surface of the airfoil. Maximum value limited to 99. Format I5

XIB(I),YIB(I) Coordinate pairs describing the lower surface of the airfoil. The leading edge corresponds to XI=0.0 and the trailing edge is XI=1.0. The vertical ordinate, YIB, is nondimensionalized by the chord. Read starting with I=1 to I=NIB. Format 8F10.4

DERIXB,DERIYB,DERFXB,DERFYB Parameters describing the leading and trailing edge of the airfoil. DERIXB is dx/ds of the airfoil lower surface at the leading edge. It is usually zero. DERIYB is dy/ds of the airfoil lower surface at the leading edge and it is usually -1.0. DERFXB is d^3x/ds^3 of the airfoil lower surface at the trailing edge. It is usually sufficiently accurate to use 0.0. DERFYB is d^3y/ds^3 of the airfoil lower surface at the trailing edge. It is usually sufficiently accurate to use 0.0. Format 4F10.4

Input Block 7: Starting Airfoil Description (Optional)

This block of data is read from subroutine FOIL and is only read if the integer input parameter IREAD is one. It effectively overwrites the information from input block six.

YU(I),YL(I),SLU(I),SLL(I) Values describing the airfoil on the starting grid. YU(I) and YL(I) are the upper and lower surface ordinates, nondimensionalized by chord, at chord location X(I). SLU(I) and SLL(I) are the upper and lower surface slopes at chord location X(I). The X(I) values depend upon the size and spacing associated with the starting grid. The group of four values is read starting at the I value corresponding to the first point downstream of the leading edge (I=ILE) and ending with the point just upstream of the trailing edge (I=ITE). Format 5E15.7

DUPOLD(I),DLWOLD(I) Values describing the boundary layer displacement thicknesses on the starting grid. DUPOLD(I) and DLWOLD(I) are the upper and lower surface displacement thicknesses corresponding to the chord location X(I). These are read starting at the I value corresponding to the first point downstream of the leading edge (I=ILE) and ending with the point just upstream of the trailing edge (I=ITE). Format 5E15.7

Input Block 8: Design Pressure Distribution (Inverse Design Mode only)

This block of data consists of four sections which are only included in the inverse design mode (INV=1). In that mode only the last three sections would usually be included.

Section 1 -- Starting solution design pressure distribution read by subroutine FOIL. This section would only be included if a design solution were being restarted (i.e. INV=1, IREAD=1, and MHALF=1) and it would only affect the first grid considered.

CPU(I) Upper surface inverse region pressure coefficient values for the design case starting with I=I1, which is the first grid point after X1 and ending with I=ITE, the grid point just upstream of the trailing edge. Format 8E10.3

CPL(I) Lower surface inverse region pressure coefficient values for the design case starting with I=I1, which is the first grid point after X1 and ending with I=ITE, the grid point just upstream of the trailing edge. Format 8E10.3

Section 2 -- This section reads in the starting and ending points of the inverse region from subroutine COORD and the inverse design pressure distribution from subroutine FOIL for the second grid. Used only in the inverse design case (INV=1).

X1,X2 X1 is the location where the direct calculation stops and the inverse calculation begins. Typically, it is slightly less than the third point from the leading edge or larger. X2 is the location where the inverse calculation stops. It should always be set to 0.5. Format 2F10.5

CPU(I) Upper surface inverse region pressure coefficient values for the design case starting with I=I1, which is the first grid point after X1 and ending with I=ITE, the grid point just upstream of the trailing edge. Format 8E10.3

CPL(I) Lower surface inverse region pressure coefficient values for the design case starting with I=I1, which is the first grid point after X1 and ending with I=ITE, the grid point just upstream of the trailing edge. Format 8E10.3

Section 3 -- This section reads in the starting and ending points of the inverse region from subroutine COORD and the inverse design pressure distribution from subroutine FOIL for the third grid. Used only in the inverse design case (INV=1). The input variables and descriptions are the same as Section 2 above.

Section 4 -- This section reads in the starting and ending points of the inverse region from subroutine COORD and the inverse design pressure distribution from subroutine FOIL for the fourth grid. Used only in the inverse design case (INV=1) when ITERP is zero. Note that in References (2) and (4), the use of grid four for inverse design is not recommended. The input variables and descriptions are the same as Section 2 above.

OUTPUT DESCRIPTION

THe printed output when the program is operated in the inverse design mode is identical to that described in Reference (4). When the program is operated in the analysis mode with the massive separation option, the output for grids two, three, and four has the form shown below. Since the first grid assumes inviscid flow only, its printout only includes those portions associated with an inviscid solution.

1. Heading (user supplied)

2. Case Number

3. Mach number and angle of attack

4. Case type callouts, i.e.,

   INVISCID ANALYSIS CASE

   WITH LAMINAR TURBULENT VISCOUS INTERACTION

   AND MASSIVE SEPARATION

   AND VARIABLE PRESSURE IN SEPARATED REGION

5. Input data in namelists FINP and IINP

6. Coordinate System for the current grid printed as I, X(I) followed by J, Y(J)

7. Ordinates of the current airfoil displacement surface

   X -- Horizontal ordinate, where -0.5 is the leading edge and 0.5 is the trailing edge

   YU -- Upper displacement surface ordinate

   YL -- Lower displacement surface ordinate

   UPPER SLOPE -- Slope of upper displacement surface

   LOWER SLOPE -- Slope of lower displacement surface

8. Iteration history at ten-cycle intervals

   CIR -- Circulation

   DPM -- Maximum φ correction (absolute value) in the last relaxation cycle with the corresponding (I,J) grid location

   NSSP -- Number of supersonic grid points

   DELTAY OR YUTE -- In the design case, the change in YU(ITE), the upper surface trailing edge ordinate, since the last surface update. Should go to zero if

converging. In the viscous analysis case, it is the current value of YU(ITE); and it should approach a constant value if the solution is converging. Only changes after the first fifty cycles on each grid.

SEP AT X -- The current x ordinate value for the upper surface separation point (x = -0.5 is the leading edge and x = 0.5 is the trailing edge).

9. Boundary Layer Information

Every LP cycles results of the current boundary layer solution are printed first for the lower surface of the airfoil and then for the upper surface. In each case, the laminar solution (if ILAM=1) is printed first followed by the turbulent solution.

9a. Laminar Boundary Layer Information (Printed every LP cycles)

X -- Horizontal ordinate

MACH # -- Local Mach number

CF -- Skin friction coefficient (the 0.1E11 initial value is arbitrary and should be ignored)

D-STAR -- δ^*/c, non-dimensional boundary layer displacement thickness

D-THETA -- θ/c, non-dimensional momentum thickness

H -- δ^*/θ shape factor

RE-THETA -- Local Reynolds number based on θ

RE-STAR -- Local Reynolds number based on δ^*

TM -- $\theta^2 (du/dx)/\nu$, Pressure gradient parameter

9b. Possible Laminar Flow Messages

a. SEPARATION OCCURRED AT X = 0.xxx -- gives x location where laminar separation occurred.

b. SHORT BUBBLE FORMED? TRANSITION TO TURBULENT FLOW ASSUMED, X= 0.xxx

c. LONG BUBBLE? LAMINAR STALL MAY OCCUR, X = 0.xxx
BOUNDARY LAYER CALCULATION WILL BE CONTINUED AS TURBULENT BUT ACCURACY OF RESULTS IS QUESTIONABLE

d. BOUNDARY LAYER CALCULATION COMPLETED?
NEITHER SEPARATION NOR TRANSITION WAS DETECTED

9c. Turbulent Boundary Layer Information (Printed every LP cycles)

X -- Horizontal ordinate (-0.5 is leading edge, 0.5 is trailing edge)

MACH # -- Local Mach number

DLSTR -- δ^*/c, non-dimensional boundary layer displacement thickness

DEL -- δ/c , non-dimensional boundary layer thicknesses

CUE -- U_e, transformed boundary layer edge velocity, $U=(a_\infty/a_e)u$

USTAR -- Law of the wall parameter, SQRT(τ_w/ρ)

USTAR**2 -- Skin friction parameter, τ_w/ρ

THETA -- θ/c, non-dimensional momentum thickness

CDP -- Profile drag coefficient using Squire-Young approach modified according to Reference (9)

CDW -- Wave drag coefficient, not computed in this version of code and thus always zero

CDTOT -- Total drag coefficient

9d. Turublent Boundary Layer Messages

a. SEPARATED CP IS 0.xxx -- In the constant separated pressure level option (IMASS=1,ITACT=1,KSEP=1) the pressure in the separated region is printed

after each boundary layer calculation. If solution is converging, it should approach a constant value.

b. USTAR2 (or USTCK) LT ZERO -- Indicates where in computation separation was first detected. See program listing for details.

10. Final Boundary Layer Results

YUORIG -- Original airfoil upper surface ordinate

DU -- Smoothed upper surface displacement thickness

SLU -- Slope of upper displacement surface

YLORIG -- Original airfoil lower surface ordinates

DL -- Smoothed lower surface displacement thickness

SLL -- Slope of lower displacement surface

11. Pressure Distribution on Airfoil

CPU -- Upper surface pressure coefficient

CPL -- Lower surface pressure coefficient

12. Final Displacement Surface Information

YU -- Ordinate of upper displacement surface

YL -- Ordinate of lower displacement surface

SLU -- Slope of upper displacement surface

SLL -- Slope of lower displacement surface

13. Mach Chart

The Mach numbers at the I,J coordinate points are multiplied by 100 and printed out in block form. The grid points "inside" the upper and lower

displacement surfaces are indicated by zeros. Velocities (U,V) at the flowfield grid points may also be printed out using option IPRT2=1.

14. Miscellaneous Information

The normal force coefficient, CN, and the drag coefficient, WAVE CD, obtained by integration of the pressure distribution are printed out. The latter should theoretically be zero for subcritical unseparated cases, but it usually is non-zero due to mesh size and grid placement. Thus values of WAVE CD should only be used for comparison purposes.

15. Printer Plot of Results

U -- Upper surface pressure coefficient

L -- Lower surface pressure coefficient

T -- Upper displacement surface

B -- Lower displacement surface

CPSTAR -- Pressure coefficient for local Mach number of one

CLCIR -- Lift coefficient from computed circulation

CL -- Lift coefficient from integration of pressure distribution

CD -- Wave drag plus profile drag coefficient (Accuracy depends upon value of CDWAVE)

CMLE -- Moment coefficient about the leading edge

CDF -- Profile drag coefficient using Squire-Young approach modified for separation and compressibility

CMC4 -- Moment Coefficient about quarter chord point

16. Miscellaneous Messages

PROD .LE. ZERO -- This message indicates that the turbulent boundary calculation was unable to obtain an appropriate starting solution. As a result the flowfield calculations were continued with the displacement surface ordinates and slopes frozen at their last updated values. This situation usually occurs when transition takes place at the shock wave and the local Mach number immediately upstream of the shock wave is greater than 1.35. It probably indicates that at a minimum there is local separation in the vicinity of the shock wave. Since this phenomena is not modeled in the present code the results obtained in such cases should be used carefully. Sometimes this problem can be "avoided" by computing an all turbulent case (ILAM=0) with transition at or immediately upstream of the shock wave. It should be noted that when this message appears, the subsequent computed values of CDF are in error.

AA .LT. ZERO -- This message occurs when the local speed of sound is computed to be negative. It indicates that either the solution has become unstable or else the rotated scheme tried to use a point outside of the solution domain due to a supersonic point on the JMAX-1 row. Usual solution is to increase the supersonic damping, EPSS, and/or increase the stretching and /or size of the Y grid. When encountered, the computation is terminated and the current perturbation flowfield solution is printed for diagnostic purposes.

17. Note that additional output can be obtained for either diagnostic or analysis purposes by removing the C's from various commented print statements in the program.

TYPICAL RESULTS

In the development of the present method, results have been obtained for NACA 4412 and NACA 0012 airfoils for freestream Mach numbers up to 0.5, angles of attack up to 18.5 degrees, and Reynolds numbers between three and nine million. These conditions were selected not because of limitations in the method but due to the availability of excellent experimental pressure distribution data in those regions.[19-21] Thus, the results presented here are only meant to be representative.

Figures 4 and 5 compare results obtained with the present method with the low speed experimental data of Pinkerton[21] for a NACA 4412 airfoil at 6.3 million Reynolds number. In Figure 4 the experimental data has been plotted using the angle of attack correction suggested in Reference 21. As can be seen, the theory predicts slightly larger lift coefficients than the data at the lower angles of attack. Whether this difference is due to an underestimation of the angle of attack correction, as suggested in Reference 22, or a problem in the theoretical model is unknown. In any event, the theory and the data are in excellent agreement between ten and fifteen degrees; and the present model reasonably predicts the location of maximum lift at an angle of attack of about 16 to 17 degrees. The theoretical model does, however, overpredict slightly (1.8 vs. 1.7) the maximum lift coefficient predicted by this forty-seven year old data.

Figure 5 compares pressure distribution results obtained with the present method with the experimental data of Pinkerton at an angle of attack slightly below that corresponding to maximum lift. In this case, the corrected angle of attack was used in the computations, and the upper and lower surface boundary

layers were assumed to be initially laminar followed by natural transtion to turbulent flow. For this high lift case, the theory predictes that the lower surface remaines entirely laminar and that the upper surface transitions at one percent chord followed by separation at 74.9 percent chord. As can be seen on the figure, the predicted pressure distribution is in excellent agreement with the data; and the pressure coefficient in the separated zone is slightly negative and constant. Experience indicates that for low speed cases better results are usually obtained using the constant pressure option (KSEP=0) for the separated zone. For this case, the theoretical lift coefficient was 1.69 while the experimental value was 1.68. The predicted profile drag coefficient was 0.0200, which is in reasonable agreement with available measurements.23

As indicated previously, it is important for this type of method to include the effects of a laminar boundary layer. Figure 6 shows lower surface laminar-turbulent transition point locations predicted by the present method for a NACA 0012 airfoil at Mach 0.3 and six million Reynolds number. As can be seen, for these flight conditions the lower surface boundary layer is predominantly laminar at low angles of attack; and at angles of attack above ten degrees it is essentially all laminar. Obviously, a method which only includes a turbulent boundary layer calculation and/or assumes transition near the leading edge might yield incorrect results for these flight conditions.

Figure 6 also shows for the same conditions the predicted upper surface separation points determined by the TAMSEP method. Notice that no upper surface separation is predicted until about 12 degrees angle of attack. After that, as the angle of attack increases, the beginning of separation moves forward on the upper surface until more than half of the airfoil experiences separated

flow at about 16 degrees. For this case, maximum lift occurs around fourteen degrees.

Figure 7 compares the predicted lift coefficient variation with angle of attack for a NACA 0012 airfoil at the same nominal conditions (i.e. Mach 0.3 and six million Reynolds number) with experimental data obtained in the Low Turbulence Pressure Tunnel at NASA Langley.[20] These data were obtained on clean airfoils without the use of trip strips, and thus the theoretical results were obtained using the laminar natural-transition turbulent model (ILAM=1). At the lower angles of attack the agreement is quite good. However, at the onset of trailing edge separation, around twelve degrees, the theoretical lift curve exhibits a "kink" accompanied by a slight decrease in lift coefficient. This "kink" is often observed in the theoretical lift curves when separation is first predicted and is due to the fact that separation is usually first detected on the coarse grid. On that grid, the first point forward of the trailing edge is about 93% chord; and, thus, when separation is first predicted on the coarse grid the separation point moves forward from the trailing edge to at least the 93 percent point, with the result that the amount of separation is overpredicted and the lift at that condition is underpredicted. Since the model only permits the separation point to move forward, this effect is maintained thoughout all the grids at that angle of attack. However, as the angle of attack is increased this effect disappears. Thus, at low and medium freestream Mach numbers, the lift coefficients predicted at angles of attack just above the onset of trailing edge separation are usually slightly low.

However, as can be seen on Figure 7, the lift coefficients predicted at the higher angles of attack are, at least for this case, in reasonable agreement with

the experimental data. Notice that for this case the experimental data indicates an apparent maximum lift around fourteen degrees followed by a decrease and then an increase. The theoretical lift based upon the calculated circulation predicts a maximum lift coefficient of about 1.40 at 14 to 16 degrees. On the other hand, the theoretical lift based upon integration of the pressure distributions indicates a maximum lift at fourteen degrees, which nominally agrees with experimental data. This slight divergence between the values predicted by circulation and those by pressure integration is, based upon experience, an excellent indication of the maximum lift location at low and medium speeds. The reason for this statement will be evident when the pressure distributions for these cases are discussed.

The predicted variation of drag with lift for this case is compared to experimental data at the higher lift coefficients on Figure 8. Again the zig-zag in the theoretical curve corresponds to the similar phenomena on the lift versus angle of attack plot and is due to the overprediction of the size of the initial separated zone. Nevertheless, the agreement between the theoretical predictions and experimental values, particularly near maximum lift, is good and should be acceptable for applied engineering calculations.

Figures 9(a-c) compare pressure distributions obtained with the present method with data obtained in the Low Turbulence Pressure Tunnel at NASA Langley[20] at three different angles of attack. The first corresponds to an unseparated flow situation, the second is near maximum lift, and the third is for an angle of attack above the maximum lift condition. Since at medium freestream Mach numbers and higher evidence[9,19-20] indicates that the pressure variation in a separated zone is not constant, these and subsequent cases were all run using

the variable pressure option (KSEP=1). As can be seen on Figure 9(a) the theoretical pressure distribution for the unseparated case is in excellent agreement with experimental data. For this case, the theoretical lift and drag coefficients were 1.27 and 0.0116 while the corresponding clean airfoil experimental values were 1.23 and 0.0123.

For the case near maximum lift, Figure 9(b), it should be noted that some supersonic flow exists over the upper surface of the airfoil in a very small region near the leading edge since the critical C_p for this case is -6.89. In addition, the theoretical method predicts upper surface separation at 74.9 percent chord and boundary layer instability on the lower surface at about 80 percent chord. However, due to the favorable pressure gradient, the lower surface boundary layer never transitions. For this case the theoretical lift coefficient of 1.39 coincides with the experimentally measured value, and the two pressure distributions exhibit reasonable agreement.

At an angle of attack greater than that corresponding to maximum lift, the flow about an airfoil is typically characterized by a large region of unsteady separated flow; and a steady state solution method such as the present one is not really applicable. Thus, the apparent lack of agreement between the present steady theory and the experimental measurements shown on Figure 9(c) is not surprising. Nevertheless, the general pattern of the pressure distribution including the existence of a large separation zone is predicted; and the predicted lift coefficient of 1.44 based upon circulation is in surprising agreement with the experimentally measured value of 1.437. However, careful examination of the solution indicates that it is not completely converged, that the theoretical lift may be oscillating slightly, and that the lift based upon pressure integration

computed at the end of a run using default parameters is only 1.27. Interestingly, results using the thin layer Navier Stokes equations[17,18] for a similar case (NACA 0012, Mach No. = 0.3, Reynolds = 1 million, angle of attack = 18 degrees) indicate a lift coefficient varying with time from 0.65 to 1.6 with a Strouhal number of 0.1; and both the theoretical and experimental pressure profiles shown on Figure 9(c) are representative of those computed at various times in the cycle with the thin layer Navier Stokes model. Thus, the present theoretical result is representative of the type of pressure distribution and lift which might exist for this condition.

Another interesting feature associated with the results shown on Figure 9(c) is that the drag coefficient predicted using the method of Reference 6 (i.e. CDF) was 0.0604 while that predicted using the method of Reference 9 (i.e. CDP) was 0.1190. Normally, these two values are in good agreement with each other. Apparently, in the present method when the maximum lift condition is exceeded the solution becomes oscillatory and not completely converged, the lift computed by pressure integration diverges from and is lower than that from circulation, and the CDF and CDP values differ significantly. It is believed that these three items can be used to determine for medium Mach numbers the angle of attack corresponding to maximum lift.

Figure 10 shows for the same NACA 0012, Mach 0.3, Reynolds number 6 million case, the displacement surfaces predicted by the present method for the upper surface region between 70 percent chord and the trailing edge at various angles of attack. Below 11.13 degrees, where the flow is unseparated, the displacement thicknesses in the trailing edge zone are relatively small. However, with the onset of separation at 12.09 degrees the thicknesses begin to increase

rapidly, and the displacement surfaces take on shapes characteristic of the flow over a stalled airfoil. It should be noticed that at an angle of attack of 16.12 degrees, the displacement surface starts to curve back towards the freestream angle prior to the trailing edge. It is believed that the displacement surfaces shown on this figure have the correct behavior and are an adequate engineering representation of the real flow.

Obviously, it would be desirable for the present method to accurately model transonic flows with and without significant trailing edge separation. Consequently, predictions obtained with TAMSEP have been compared with data obtained in the NASA 8 Ft. Transonic Pressure Tunnel by Harris.[19] This data probably represents the best high lift transonic experimental airfoil data available today, and it has been used by many investigators. However, in most cases previous studies have compared results using the tunnel geometric angle of attack values and have ignored the known corrections associated with this data. Since such comparisons could lead to erroneous conclusions, the present results were obtained by matching the tunnel Mach and Reynolds numbers and using the corrected angles of attack suggested by Harris.

Figure 11 shows a transonic separated flow result compared with data obtained by Harris.[19] While the pressure distribution shown was obtained using the laminar-turbulent boundary layer option, indistinguishable results were obtained assuming transition at six percent chord. In the actual experiment, boundary layer trip strips were located at five percent chord. For this case, the present method predicts upper surface separation at 87 percent chord and lower surface transition very near the trailing edge. While the experimental shock location is slightly forward of the theoretical value and while the experimental

pressures in the trailing edge region are slightly lower than those predicted by the theory, the overall agreement is probably acceptable for engineering studies. For this case, the measured normal force coefficient was 0.994 while the predicted lift coefficient was 0.981.

A lift versus angle of attack curve typical of those predicted by the present method is compared with experimental data on Figure 12. For this freestream Mach number of 0.5, significant transonic flow accompanied by a strong shock wave is present on the upper surface at angles of attack greater than six degrees. As can be seen, the theoretical prediction, which was obtained assuming transition at six percent chord, agrees well with the experimental data up to about 7.35 degrees. Above that angle of attack, the present method predicts a maximum lift coefficient of 1.09 at 8.24 degrees with no trailing edge separation. At 9.21 degrees the theory predicts a decrease in lift coefficient to 0.982 with upper surface separation at 87 percent chord. The experimental data, however, indicates that maximum lift is 1.02 at 9.21 degrees and that trailing edge separation probably started at about 7.5 degrees. Examination of the theoretical results at 7.35 degrees reveals that the local Mach number immediately upstream of the upper surface shock wave is 1.42. Such a strong shock wave, whose strength increases with angle of attack, should induce significant shock boundary layer interaction which, unfortunately, is not modeled in the present theory and code. Therefore, in this case the differences between the theoretical results and the experimental data near maximum lift are probably due to shock boundary layer interaction and its subsequent effect on boundary layer growth and trailing edge separation. Nevertheless, the present model and code does give a reasonable indication of the location and magnitude of the maximum lift coefficient.

A similar lift curve for a freestream Mach number of 0.55 is shown on Figure 13. As before, the theoretical results were obtained using an all turbulent boundary layer; and in this case no upper surface trailing edge separation was detected until an angle of attack of 8.266 degrees. The maximum lift coefficient was computed to be 1.02 at 7.29 degrees as compared to the experimental values of 0.983 and 8.266 degrees. For this case significant transonic flow existed at all angles of attack above 4.5 degrees and by 7.29 degrees the Mach number at the upper surface shock wave had increased to 1.50. At 9.33 degrees a complete solution could not be obtained with the present method. On the medium grid the upper surface flow separated at 87 percent chord, and on the fine grid the separation point moved forward to the shock wave at about 18 percent chord and the solution failed. Quite obviously significant shock boundary layer interaction exists at these high angles of attack and the decrease in lift or stall is probably due more to shock induced separation than to the onset of significant trailing edge separation.

Nevertheless, the present method can be used to estimate reasonably accurately the occurence of this situation. As can be seen on Figure 13, the method predicts reasonably well the magnitude of the maximum lift coefficient and is conservative as to the corresponding angle of attack location. In addition, by noting the mechanism of code "failure", in this case sudden separation at the shock wave, a user can probably determine the type of stall phenomena present.

Theoretical pressure distribution results are compared with experimental data for a freestream Mach number 0.6 case in Figure 14. This case at a corrected angle of attack of 5.59 degrees and three million Reynolds number is significant for a variety of reasons. First, it is an example of a transonic case with a strong

upper surface shock wave. Second, the flow is unseparated and the data should serve as a good test of the present method for a situation without separation. Finally, this case has also been solved by Anderson et al[17] using both an Euler boundary layer method and a thin layer Navier Stokes method.

It should be noticed that the present results, like those of Anderson, agree very well with the experimental pressure distribution with respect to shock location and pressure levels. Also, for this case the experimental lift coefficient was 0.781. The present TAMSEP method predicted 0.809, the Euler boundary layer method of Anderson yielded 0.804, while his thin layer Navier Stokes result was 0.793. Obviously, the present method is capable of yielding excellent results that are in agreement with experimental data and other analytical methods. However, since it is a non-conservative full potential method, it should obtain such results with accurate shock wave locations more easily and faster than other more complicated methods.

Another lift versus angle of attack comparison is shown on Figure 15 for the NACA 0012 at a freestream Mach number of 0.6 and a Reynolds number of nine million. As can be seen the highest theoretical point plotted is at a lift coefficient value of 0.945 and an angle of attack of 6.392 degrees. At 7.348 degrees the boundary layer solution became frozen (i.e. PROD.LE.ZERO) on the medium grid due to shock boundary layer interaction, and on the fine grid the flow separated at the shock wave and a converged solution was not obtained. At 8.371 degrees the flow separated at the upper surface shock wave on the coarse grid, and again a converged solution was not obtained. For these cases, computed local Mach numbers in the vicinity of the shock wave were as high as 1.56. Thus, the theory indicates that above 6.392 degrees significant shock boundary layer

interaction probably accompanied by separation exists and that the maximum lift coefficient occurs at that angle of attack. As can be seen on the figure, the magnitude of the predicted maximum lift coefficient is in good agreement with the experimental data; although the angle of attack location is again conservative.

Based upon the results presented in this section, it is believed that the present method and code can be used at low and medium Mach numbers to accurately predict lift and pressure distributions at angles of attack up to that associated with maximum lift. At transonic speeds, the method should give good results for unseparated flows and for flows having trailing edge separation without significant shock boundary layer interaction. Thus, at transonic conditions, the method is probably currently limited, for accurate results, to Reynolds numbers of three million and higher and to local upper surface Mach numbers less than 1.4 to 1.45. In addition, it should yield reasonable estimates for the maximum lift coefficient at transonic speeds while being conservative as to the corresponding value of angle of attack; and the method should indicate the onset of significant shock boundary layer interaction.

CONCLUSION

A direct-inverse technique based upon a nonconservative full potential inviscid method, a Thwaites laminar boundary layer technique, and the Barnwell turbulent momentum integral method has been developed. This method is suitable for predicting the subsonic and transonic flowfield about airfoils having trailing edge separated flow. Extensive comparisons with experimental data indicate that the method should be a useful tool for applied aerodynamic engineering analyses. In addition, it is believed that the range of applicability of the method could be extended significantly by the addition of a shock boundary layer interaction mode.

REFERENCES

1. Carlson, L. A., "Transonic Airfoil Flowfield Analysis Using Cartesian Coordinates," NASA CR-2577, August 1975.

2. Carlson, L. A., "Transonic Airfoil Design Using Cartesian Coordinates," NASA CR-2578, April 1976.

3. Bauer, F., Garabedian, P., Korn, D., and Jameson, A., Supercritical Wing Sections II., New York., Springer-Verlag, 1975.

4. Carlson, L. A., "TRANDES: A Fortran Program for Transonic Airfoil Analysis and Design," NASA CR-2821, June 1977.

5. Barnwell, R. W., "Two Inviscid Computational Simulations of Separated Flow about Airfoils", AIAA Paper 76-379, July 1976.

6. Carlson, L. A., "TRANSEP:A Program for High Lift Separated Flow about Airfoils," NASA CR-3376, December 1980.

7. Carlson, L. A., "A Direct-Inverse Technique for Low Speed High Lift Airfoil Flowfield Analysis," AGARD CP-291, pp. 26-1 -- 26-10, February 1981.

8. Blascovich, J. D., "Characteristics of Separated Flow Airfoil Analysis Methods," AIAA Paper 84-0048, January 1984.

9. Barnwell, R. W., "A Potential-Flow/Boundary Layer Method for Calculating Subsonic and Transonic Airfoil Flow with Trailing Edge Separation," NASA TM-81850, June 1981.

10. Dvorak, F. A. and Choi, D. H.,"Separation Model for Two-Dimensional Airfoils in Transonic Flow," AIAA Journal, Vol. 22, No. 8, August 1984, pp. 1064-1070.

11. Taverna, F., " Prediction of Subsonic/Transonic Separated Flow About Airfoils," AIAA Paper 85-0205, January 1985.

12. Rizzi, A. and Viviand, H., editors, Numerical Methods for the Computation of Inviscid Transonic Flows with Shock Waves, Vieweg, 1981.

13. Salas, M. D. and Bumber, C. R., "Breakdown of the Conservative Potential Equation," AIAA Paper 85-0367, January 1985.

14. Schlichting, H., Boundary Layer Theory, 6th ed., New York, McGraw-Hill, 1968, p. 479.

15. Maskew, B. and Dvorak, F. A., "Investigation of Separation Models for the Prediction of C_{Lmax}, AHS Paper 77-33-01, May 1977.

16. Henderson, M. L., "A Solution to the 2-D Separated Wake Modeling Problem and its Use to Predict C_{Lmax} of Arbitrary Airfoil Sections, " AIAA Paper No. 78-156, January 1978.

17. Anderson, W. K., Thomas, J. L., and Rumsey, C. L., "Application of Thin-Layer Navier-Stokes Equations Near Maximum Lift," AIAA 84-0049, January 1984.

18. Rumsey, C. L, "Time-Dependent Navier-Stokes Computations of Separated Flows Over Airfoils", AIAA-85-1684, July 1985.

19. Harris, C. D., "Two-Dimensional Aerodynamic Characteristics of the NACA 0012 Airfoil in the Langley 8-Foot Transonic Pressure Tunnel," NASA TM-81927, April 1981.

20. Ladson, C.L., Private Communication, NASA Langley.

21. Pinkerton, R. M., "The Variation with Reynolds Number of Pressure Distribution over an Airfoil Section," NACA Report 613, 1938.

22. Coles, D. and Wadcock, A., "A Flying-Hot-Wire Study of Two-Dimensional Mean Flow Past an NACA 4412 Airfoil at Maximum Lift," AIAA 78-1196, July 1978.

23. Abbot, I.H. and Von Doenhoff, A. E., Theory of Wing Sections, Dover, New York, 1959, p. 489.

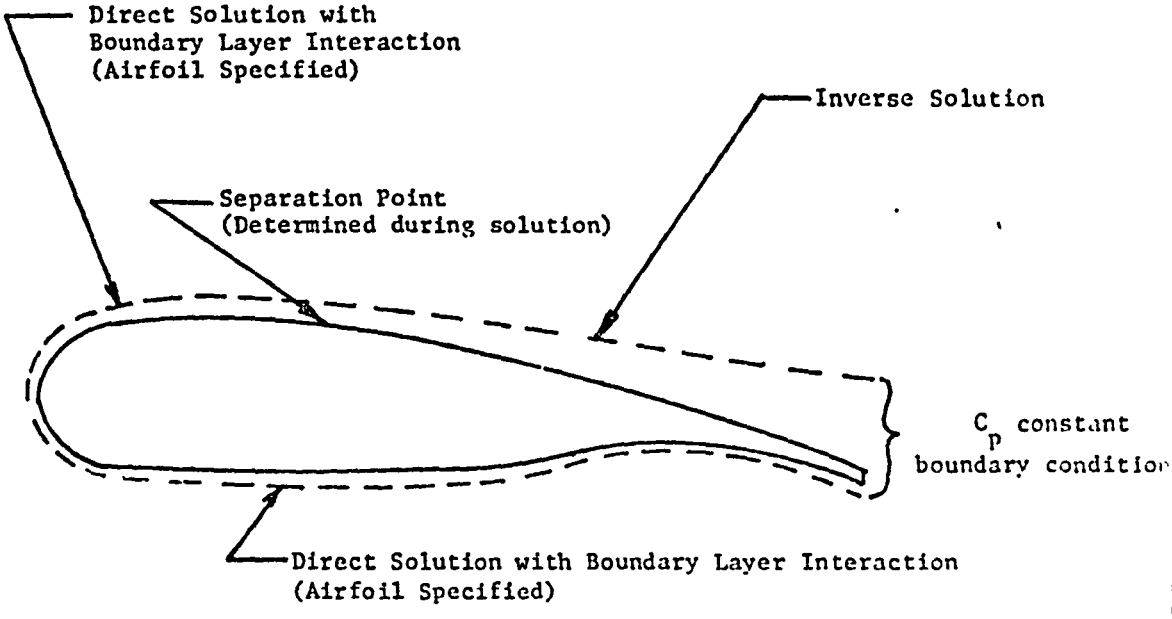

Figure 1 -- Problem Formulation

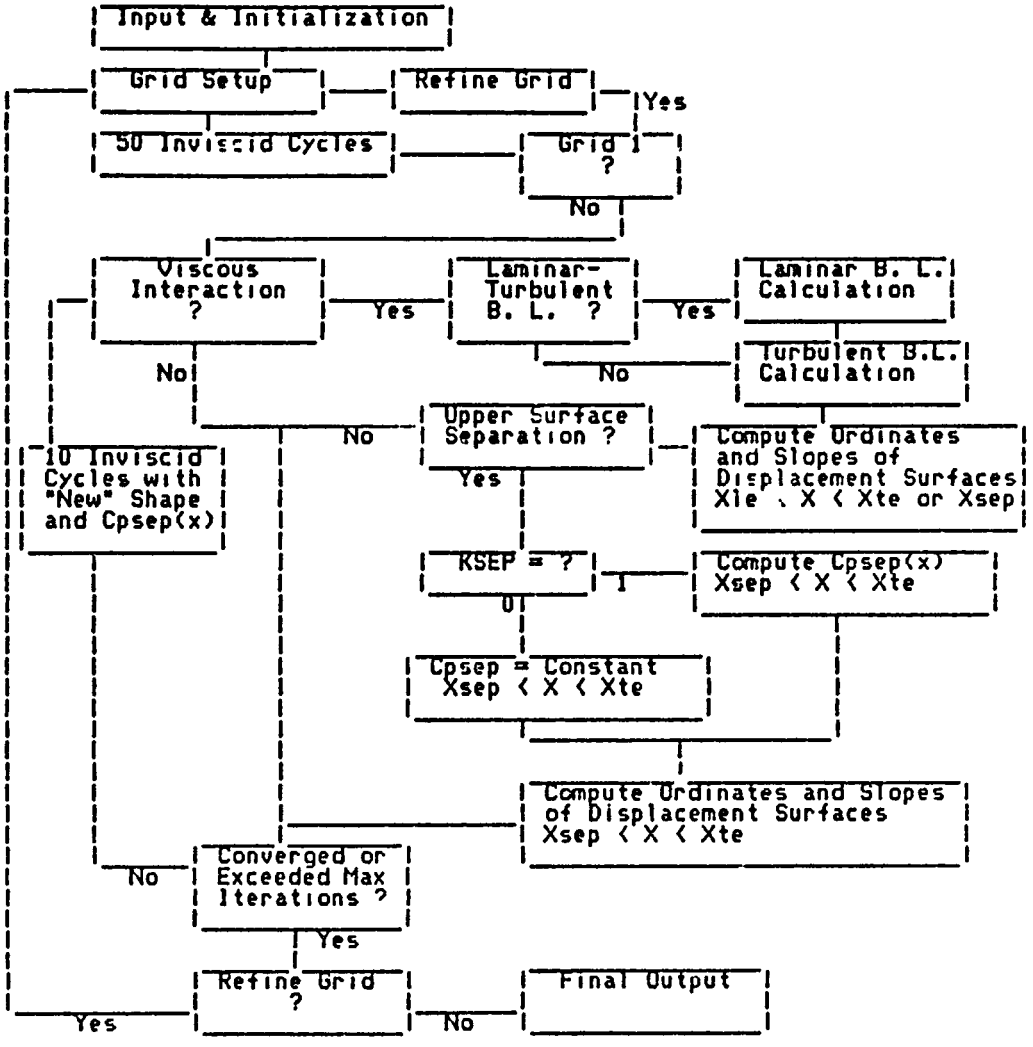

Figure 2 -- Iteration and Interaction Procedure Used in TAMSEP

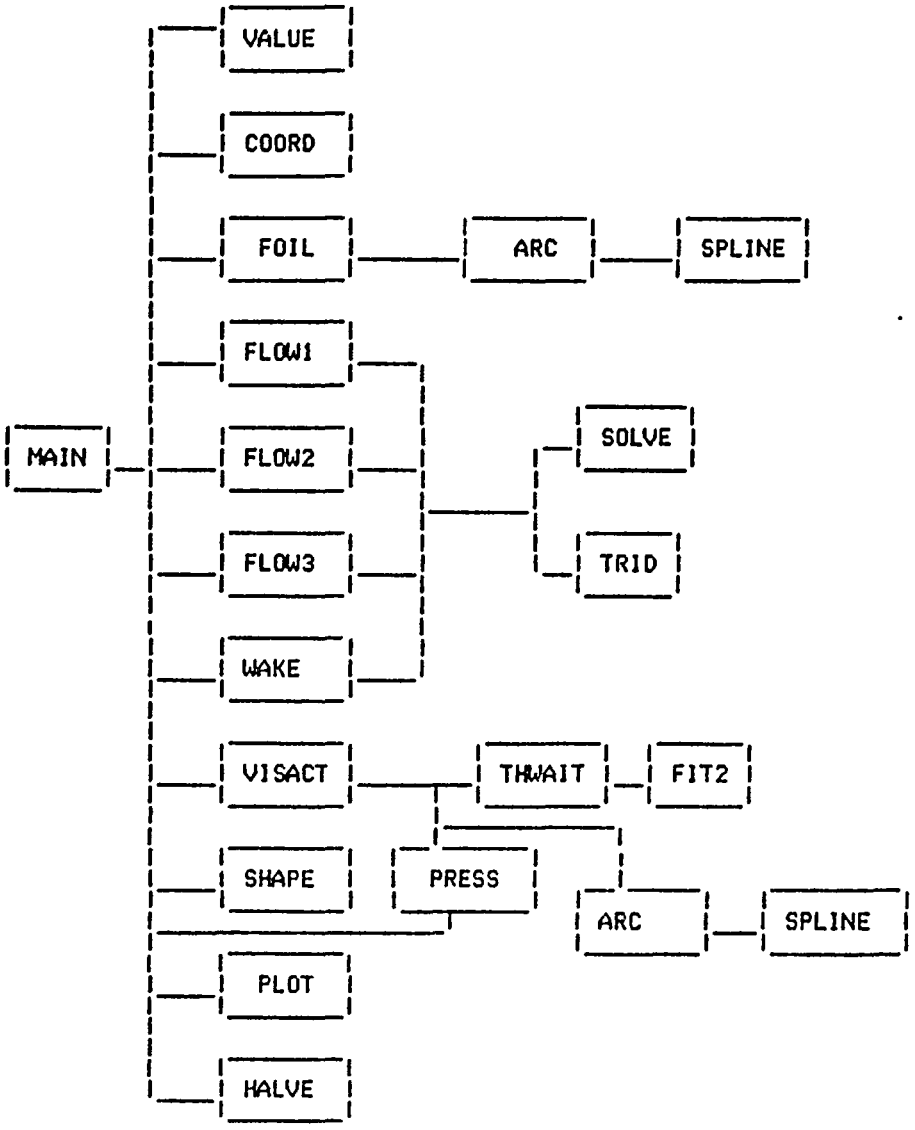

Figure 3 -- Subroutine Tree for TAMSEP

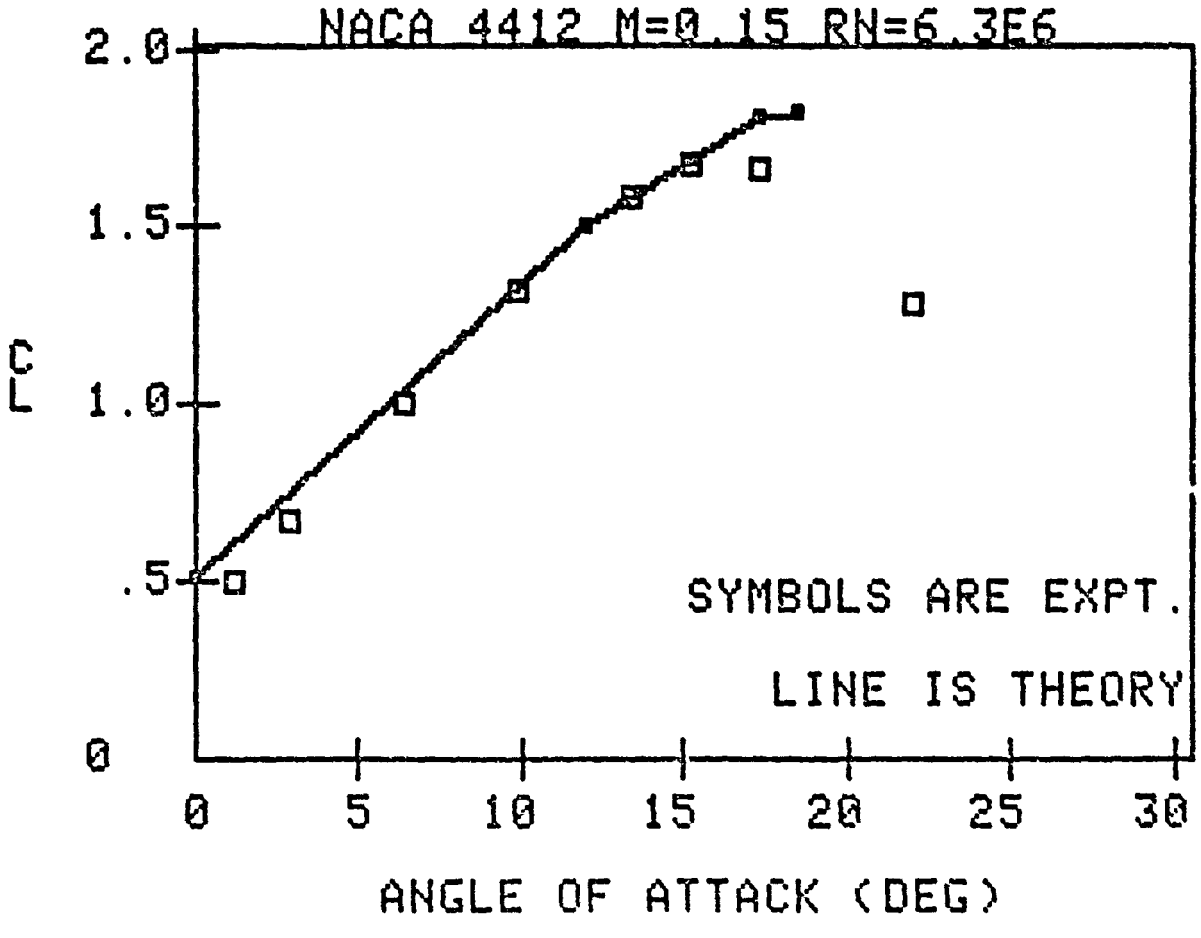

Figure 4 -- Comparison of Predicted Lift Coefficient with Experimental Data
NACA 4412 Case

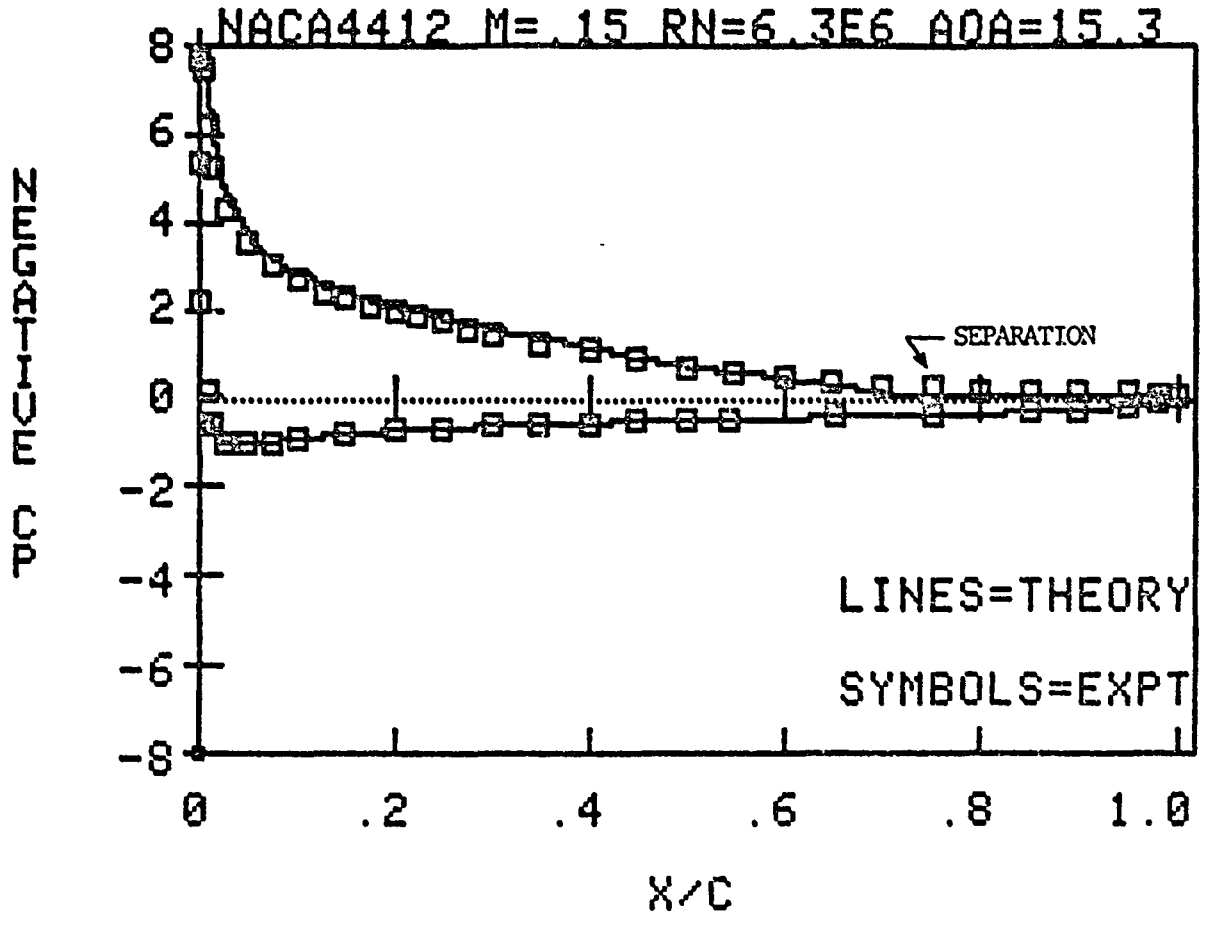

Figure 5 -- Comparison of Theoretical Pressure Distribution with Experimental Data
NACA 4412 Case

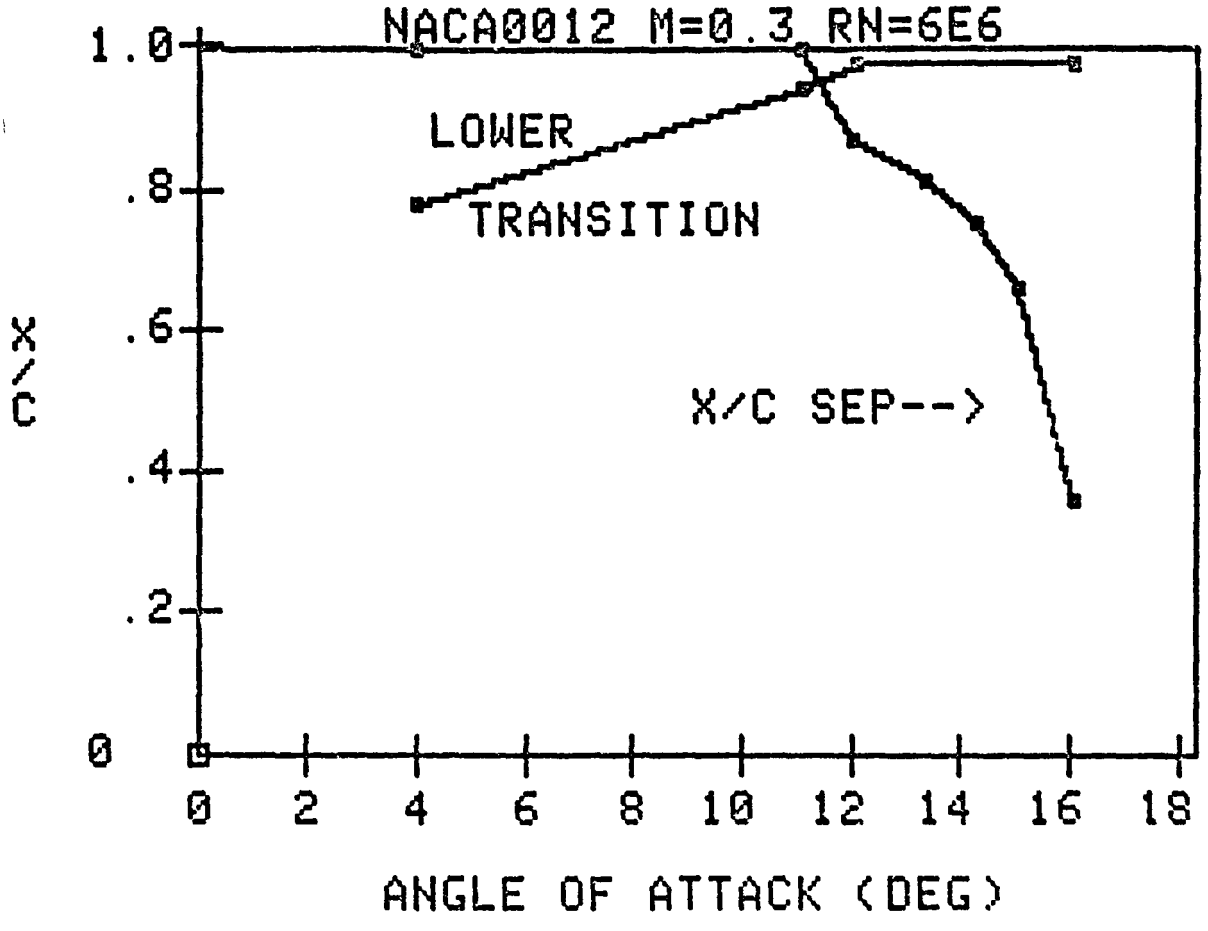

Figure 6 -- Lower Surface Transition and Upper Surface Separation Locations
NACA 0012 Case

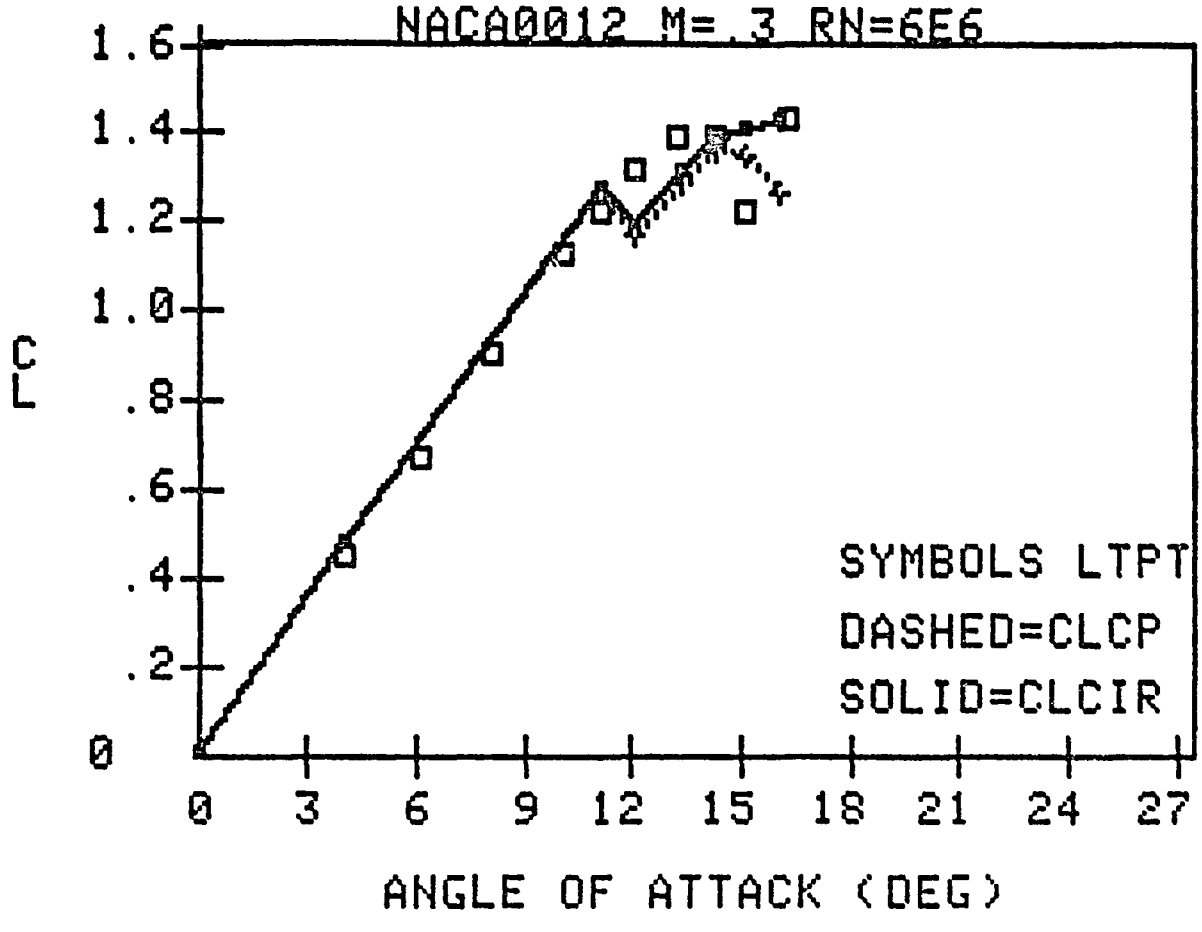

Figure 7 -- Comparison of Predicted Lift Coefficient with Experimental Data
NACA 0012 Mach No. = 0.3 Case

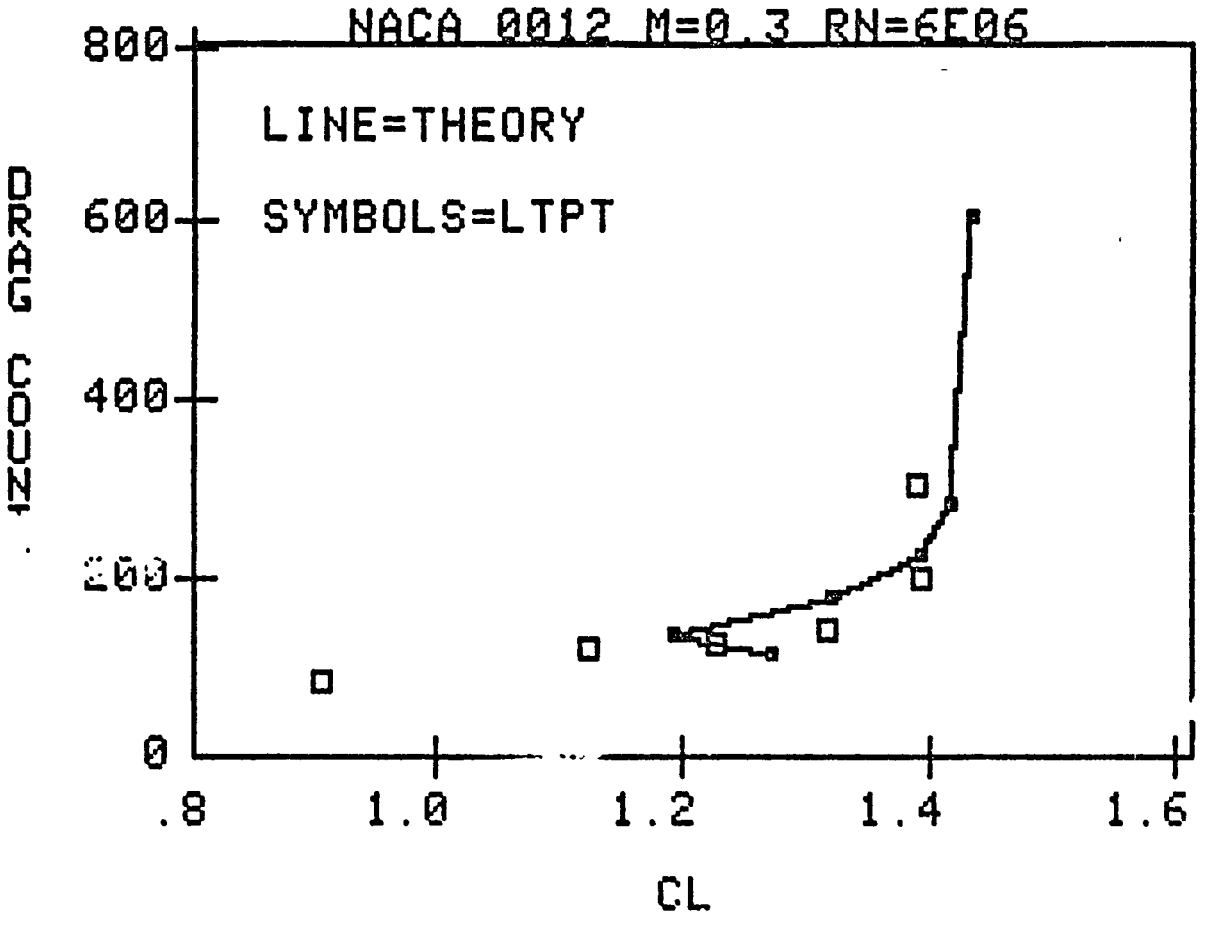

Figure 8 -- Comparison of Theoretical Lift and Drag with Experimental Data
NACA 0012 Mach No. = 0.3 Case

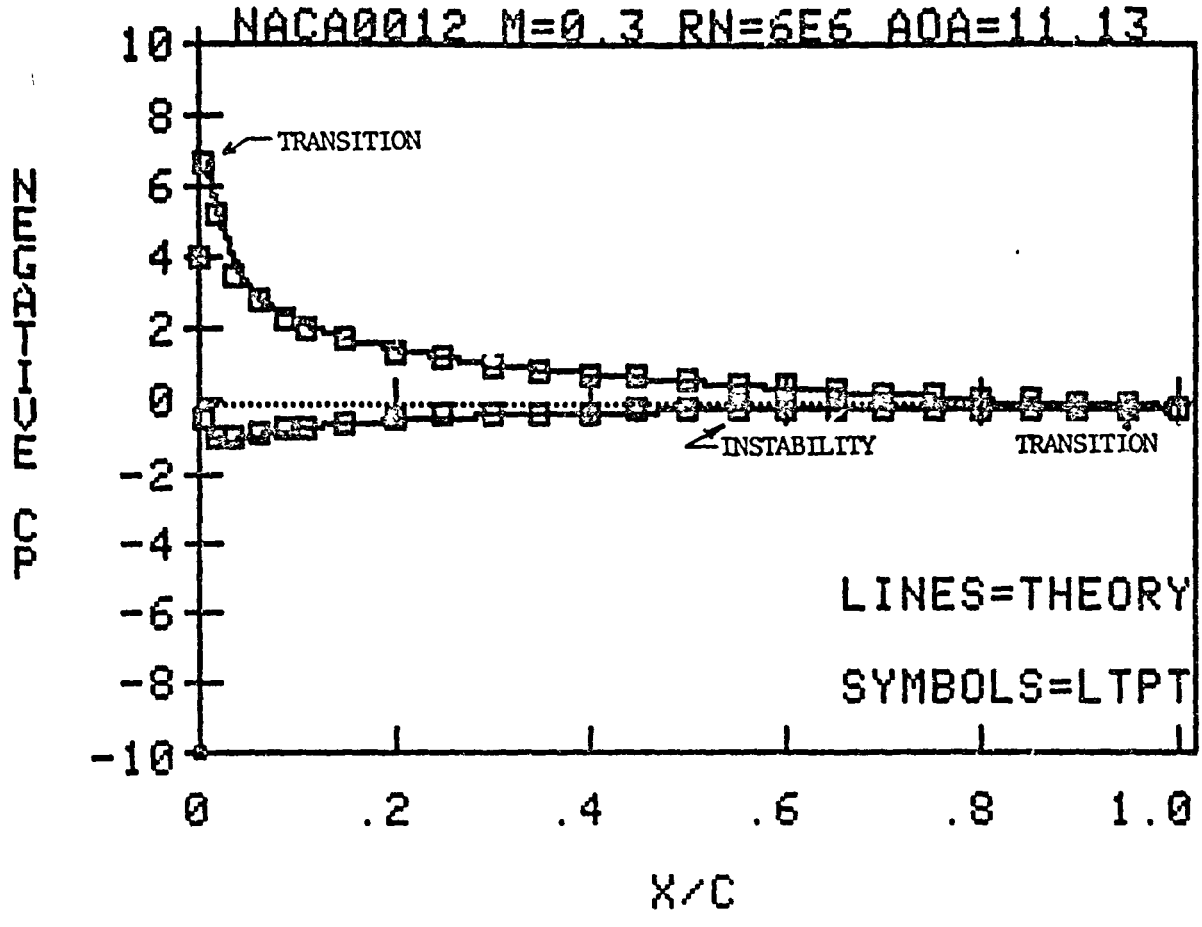

Figure 9(a) -- Theoretical and Experimental Pressure Distribution Comparisons
NACA 0012 at 11.13 Degrees Angle of Attack

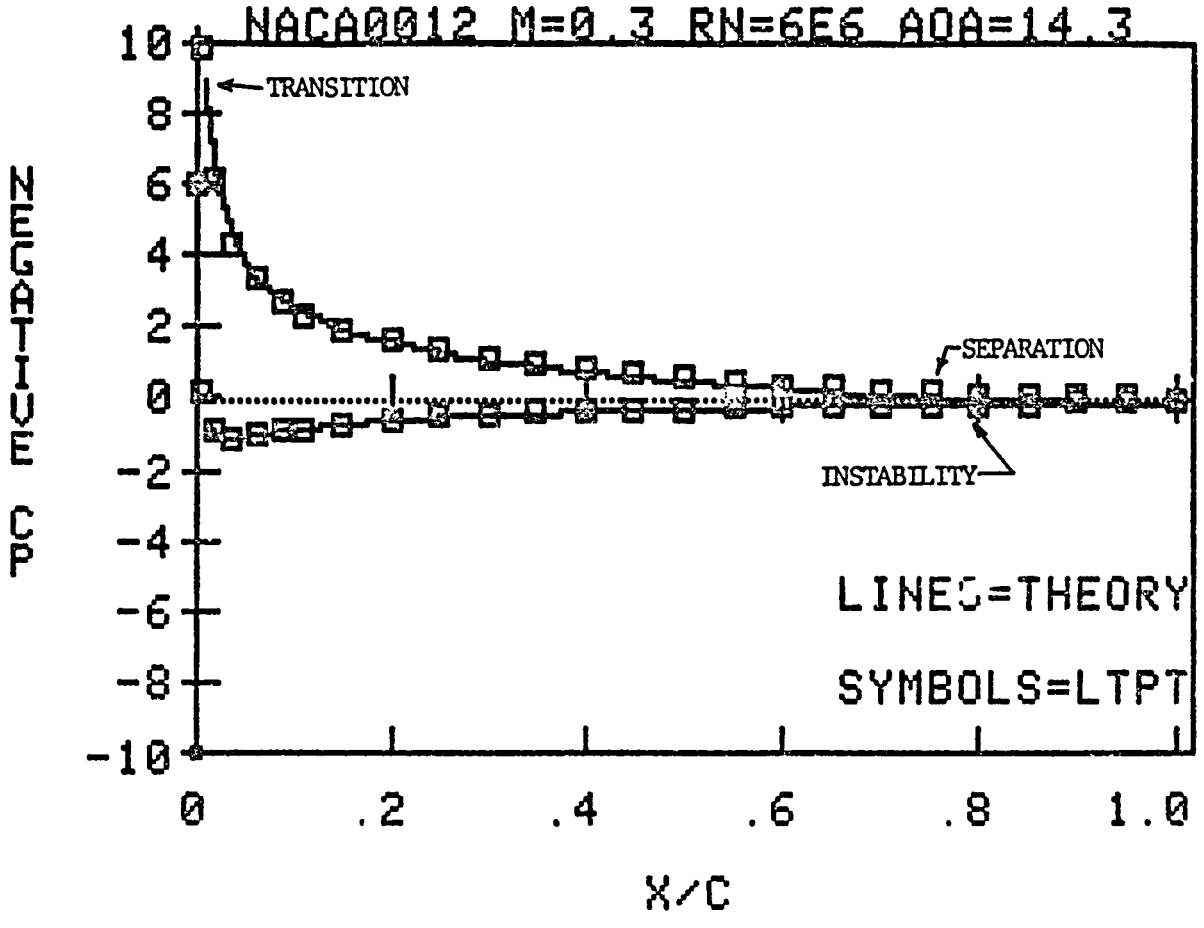

Figure 9(b) -- Theoretical and Experimental Pressure Distribution Comparisons
NACA 0012 at 14.3 Degrees Angle of Attack

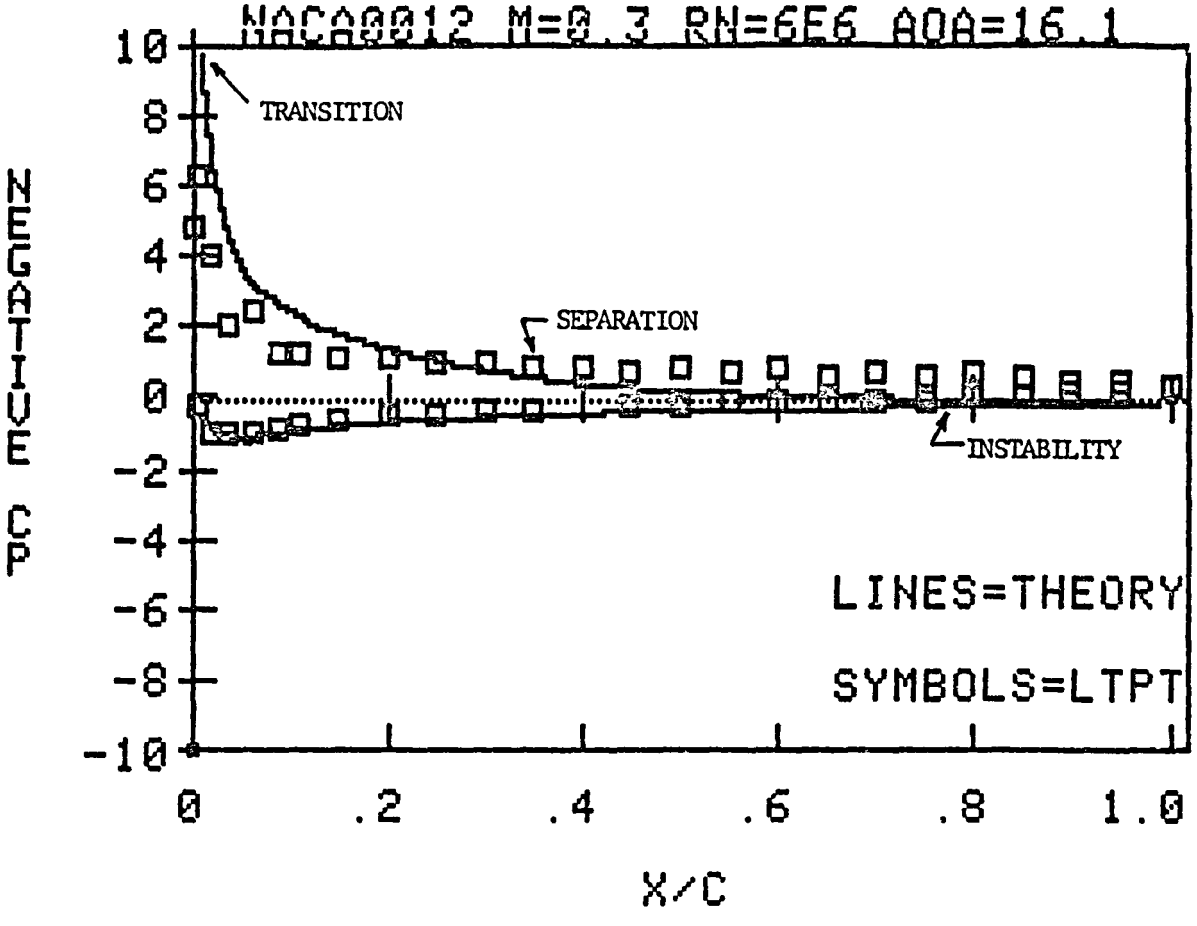

Figure 9(c) -- Theoretical and Experimental Pressure Distribution Comparisions
NACA 0012 at 16.1 Degrees Angle of Attack

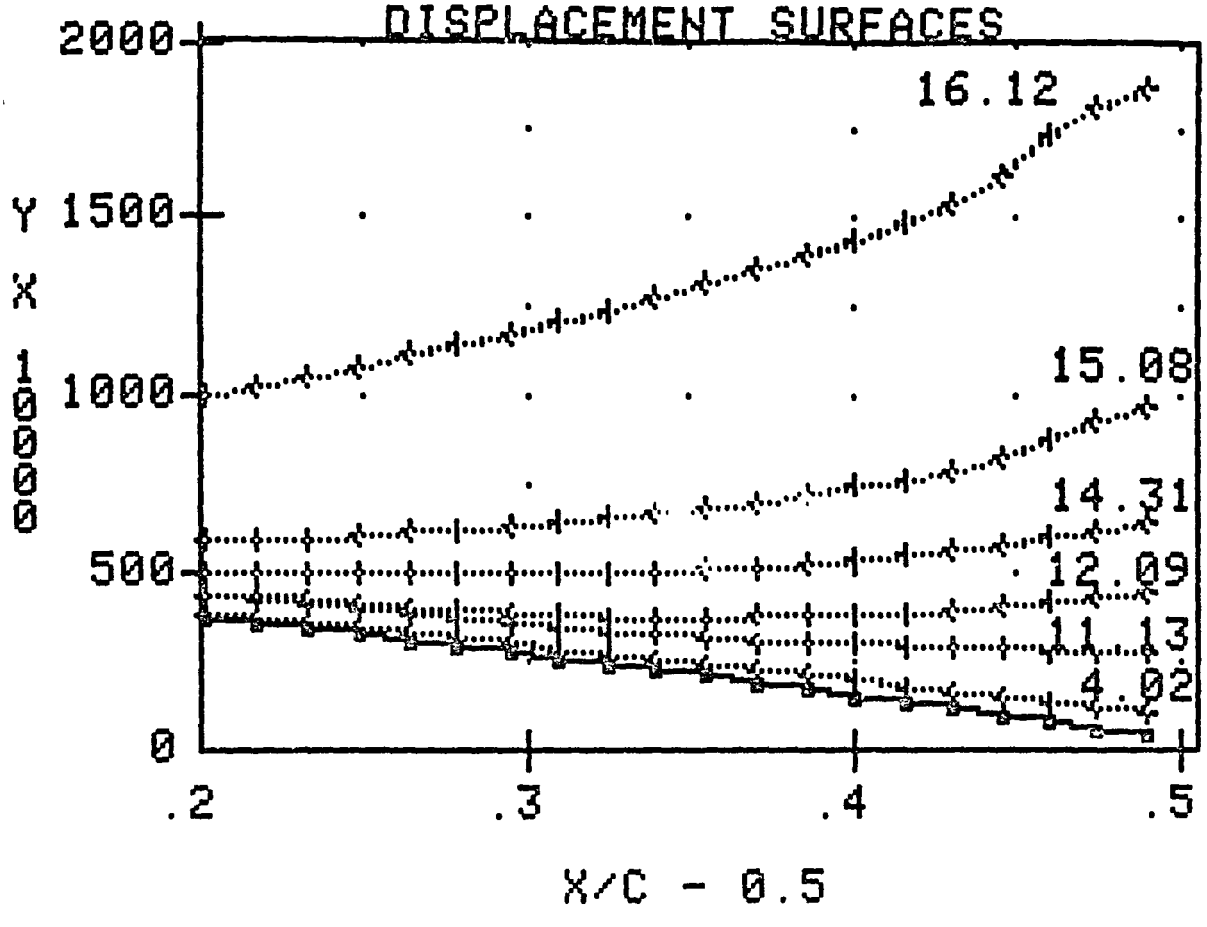

Figure 10 -- Predicted Displacement Surfaces for NACA 0012 at a Mach No. of 0.3

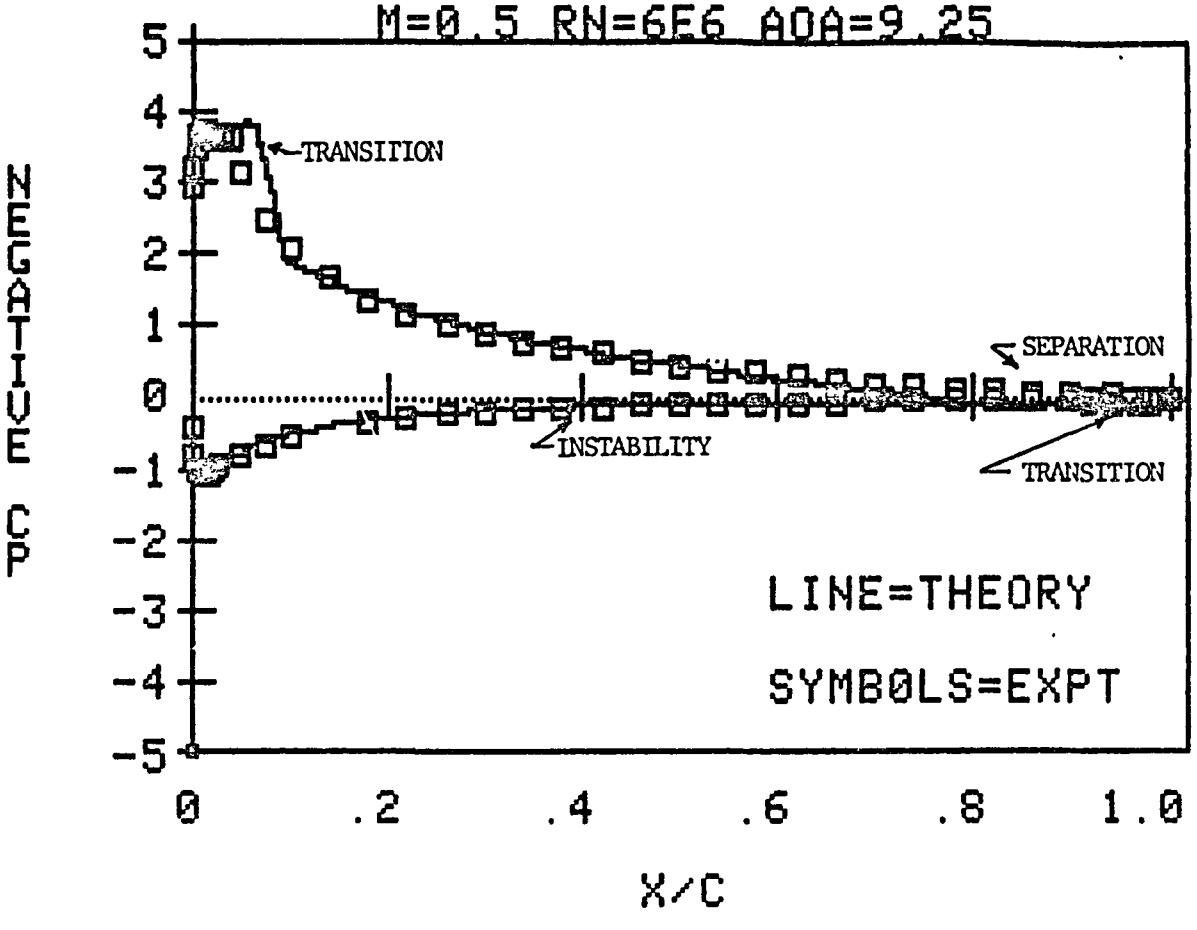

Figure 11 -- Theoretical and Experimental Pressure Distribution Comparison
NACA 0012 at Mach No. 0.5

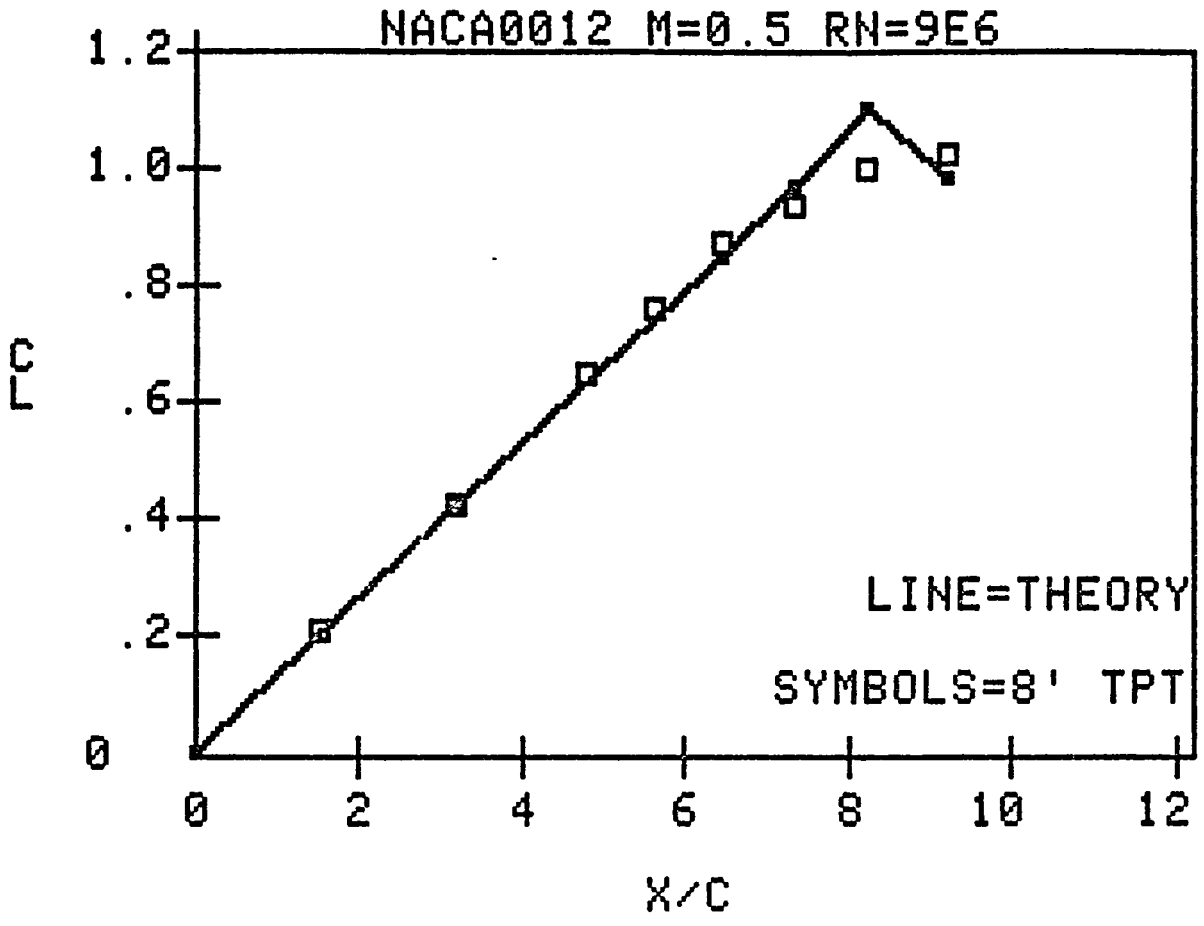

Figure 12 -- Comparison of Predicted Lift Coefficient with Experimental Data
NACA 0012 Mach No. = 0.5 Case

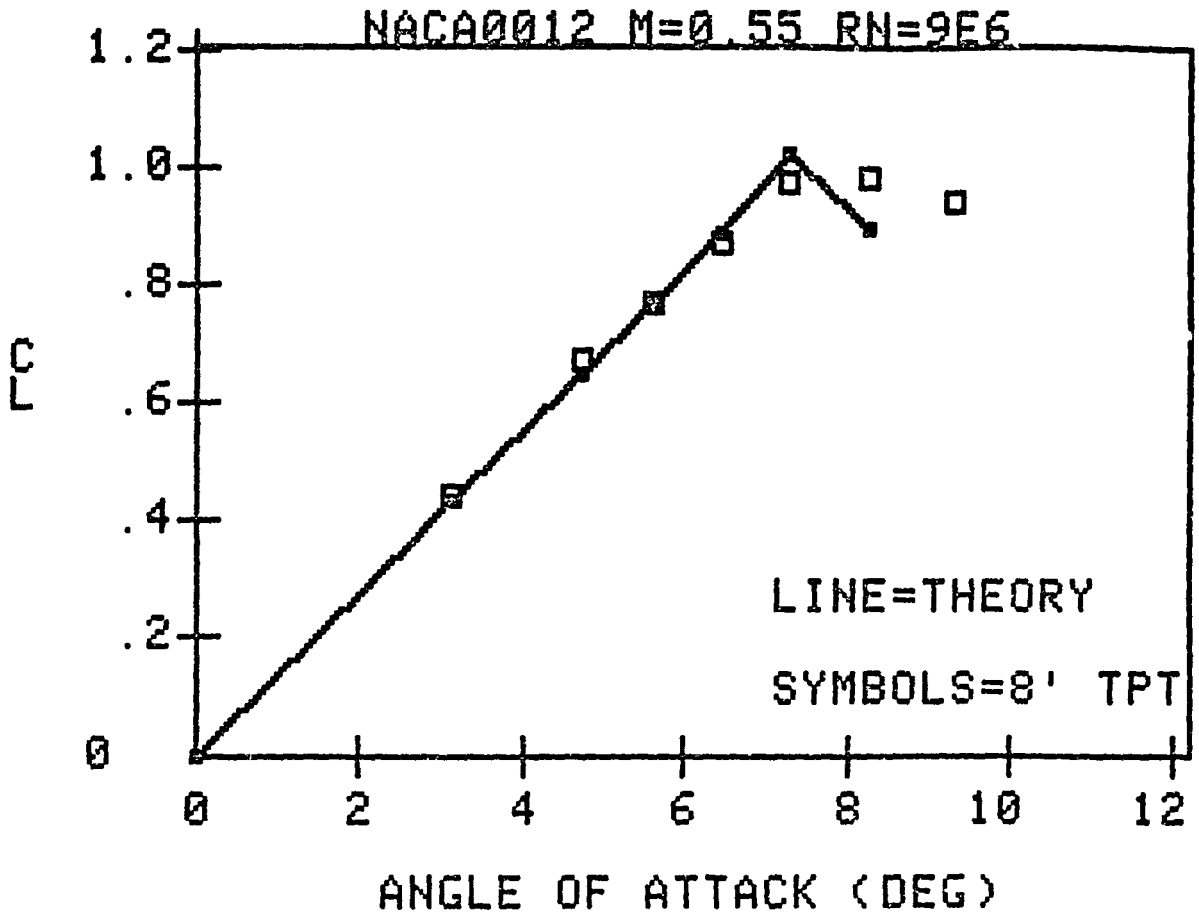

Figure 13 -- Comparison of Predicted Lift Coefficient with Experimental Data
NACA 0012 Mach No. = 0.55 Case

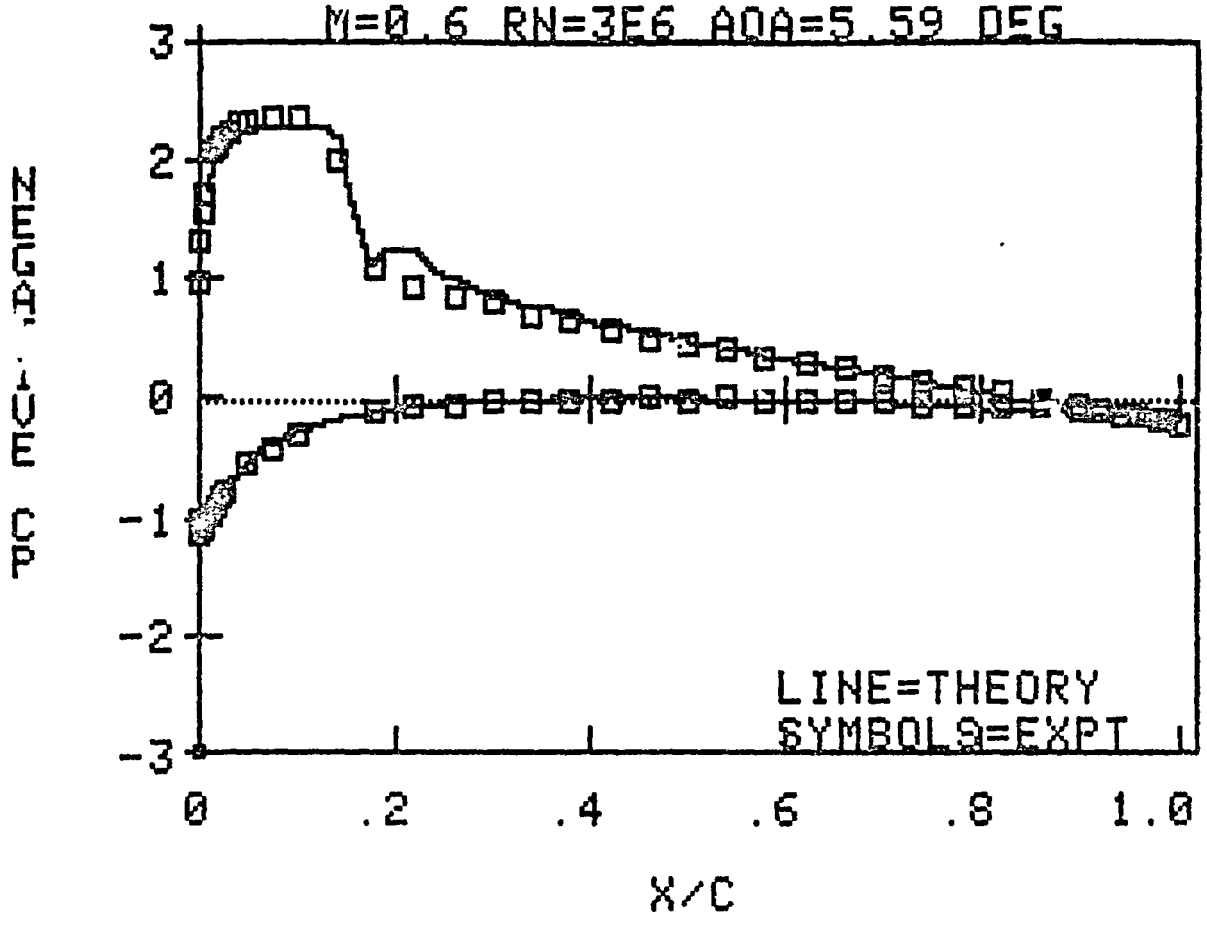

Figure 14 -- Theoretical and Experimental Pressure Distribution Comparison
NACA 0012 at Mach No. 0.6

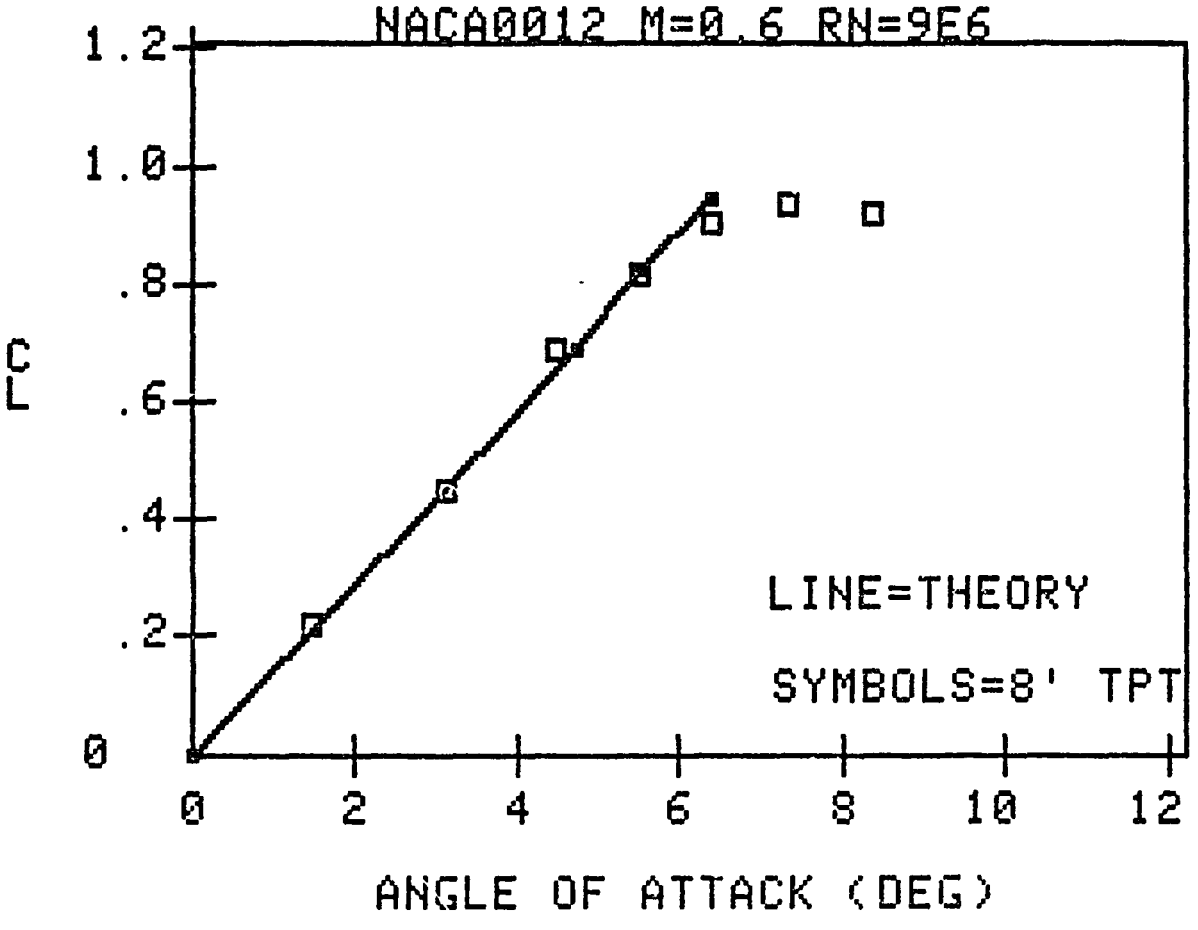

Figure 15 -- Comparison of Predicted Lift Coefficient with Experimental Data
NACA 0012 Mach No. = 0.6 Case

APPENDIX A

Sample Case Input and Output

```
TEST CASE, NACA 0012, MACH 0 5, RN 6 MILLION, ALPHA 9.25 DEG
&FINP  M=0 501,ALP=9 250,RN=6 00+06,
  EPSS=1 ,XPC= 5,&END
&IINP  IKASE=509,NHALF=2,&END
  96
 0 0        0 0        0 002500   0 008717   0 005000   0 012213   0 007500   0 014849
 0 010000   0 017037   0 012500   0 018939   0 015000   0 020637   0 017500   0 022179
 0 020000   0 023598   0 025000   0 026147   0 037500   0 031374   0 050000   0.035547
 0 062500   0 039027   0 075000   0 041999   0 087500   0 044575   0 100000   0 046828
 0.112500   0 048808   0 125000   0 050554   0 137500   0 052094   0.150000   0 053452
 0 162500   0 054644   0 175000   0 055688   0.187500   0 056594   0 200000   0 057375
 0 212500   0 058040   0 225000   0 058596   0 237500   0 059052   0.250000   0 059412
 0 262500   0.059684   0 275000   0 059873   0 287500   0 059982   0.300000   0 060017
 0 312500   0 059982   0 325000   0 059879   0 337500   0 059713   0 350000   0.059486
 0 362500   0 059202   0 375000   0 058863   0 387500   0 058471   0 400000   0.058030
 0 412500   0 057541   0 425000   0 057006   0 437500   0 056428   0 450000   0 055807
 0 462500   0 055147   0 475000   0 054448   0 487500   0 053712   0 500000   0 052940
 0 512500   0 052134   0 525000   0 051296   0 537500   0 050425   0 550000   0 049524
 0 562500   0 048594   0.575000   0 047634   0 587500   0 046647   0 600000   0 045634
 0 612500   0 044594   0 625000   0 043529   0 637500   0.042439   0 650000   0 041325
 0 662500   0 040188   0 675000   0 039027   0 687500   0.037844   0 700000   0 036639
 0 712500   0 035412   0.725000   0 034164   0 737500   0 032894   0 750000   0 031603
 0 762500   0 030291   0 775000   0 028959   0 787500   0 027605   0 800000   0 026231
 0 812500   0 024836   0 825000   0 023420   0 837500   0 021984   0 850000   0 020526
 0 862500   0 019016   0 875000   0 017545   0 887500   0 016022   0 900000   0 014477
 0 912500   0 012909   0 925000   0.011318   0 937500   0 009704   0 950000   0 008066
 0 962500   0 006402   0 975000   0 004714   0 977500   0 004374   0 980000   0 004032
 0 982500   0 003689   0 985000   0 003345   0 987500   0 003000   0 990000   0 002654
 0 992500   0 002307   0 995000   0 001959   0 997500   0 001610   1 000000   0 001260
     0 0        1 0        0 0        0 0
  96
 0 0        0 0        0 002500  -0 008717   0 005000  -0 012213   0 007500  -0 014819
 0 010000  -0 017037   0 012500  -0 018939   0 015000  -0 020637   0 017500  -0 022179
 0 020000  -0 023598   0 025000  -0 026147   0 037500  -0 031374   0 050000  -0 035547
 0 062500  -0 039027   0 075000  -0 041999   0 087500  -0 044575   0 100000  -0 046828
 0 112500  -0 048808   0 125000  -0 050554   0 137500  -0 052094   0 150000  -0 053452
 0 162500  -0 054644   0 175000  -0 055688   0 187500  -0 056594   0 200000  -0 057375
 0 212500  -0 058040   0 225000  -0 058596   0 237500  -0 059052   0 250000  -0 059412
 0 262500  -0 059684   0 275000  -0 059873   0 287500  -0 059982   0 300000  -0 060017
 0 312500  -0 059982   0 325000  -0 059879   0 337500  -0 059713   0 350000  -0 059486
 0 362500  -0 059202   0 375000  -0 058863   0 387500  -0 058471   0 400000  -0 058030
 0 412500  -0 057541   0 425000  -0 057006   0 437500  -0 056428   0 450000  -0 055807
 0 462500  -0 055147   0 475000  -0 054448   0 487500  -0 053712   0 500000  -0 052940
 0 512500  -0 052134   0 525000  -0 051296   0 537500  -0 050425   0 550000  -0 049524
 0 562500  -0 048594   0 575000  -0 047634   0 587500  -0 046647   0 600000  -0 045634
 0 612500  -0 014594   0 625000  -0 043529   0 637500  -0 042439   0 650000  -0 041325
 0 662500  -0 040188   0 675000  -0 039027   0 687500  -0 037814   0 700000  -0 036639
 0 712500  -0 035412   0 725000  -0 034161   0 737500  -0 032894   0 750000  -0 031603
 0 762500  -0 030291   0 775000  -0 028959   0 787500  -0 027605   0 800000  -0 026231
 0 812500  -0 024836   0 825000  -0 023420   0 837500  -0 021984   0 850000  -0 020526
 0 862500  -0 019046   0 875000  -0 017515   0 887500  -0 016022   0 900000  -0 014477
 0 912500  -0 012909   0 925000  -0 011318   0 937500  -0 009704   0 950000  -0 008066
 0 962500  -0 006402   0 975000  -0 004714   0 977500  -0 004374   0 980000  -0 004032
 0 982500  -0 003689   0 985000  -0 003345   0 987500  -0 003000   0 990000  -0 002654
 0 992500  -0 002307   0 995000  -0 001959   0 997500  -0 001610   1 000000  -0 001260
     0 0       -1 0        0 0        0 0
```

```
TEST CASE, NACA 0012  MACH 0.8, RN 9 MILLION, ALPHA 0.25 DEG

                    CASE NUMBER   800

          MACH NO  IS 0.80 ANGLE OF ATTACK IS   0.250 DEGREES

                    INVISCID ANALYSIS CASE
                    WITH LAMINAR TURBULENT VISCOUS INTERACTION
                    AND MASSIVE SEPARATION
                    AND VARIABLE PRESSURE IN SEPARATED REGION

$FIND
M=  .800000007    ,W=  1.00000001    ,RI=  .000000000    ,RI=  10000.0000    ,ALP=  .1016403675    ,EPS=  0.            ,EPS0=
  1.00000000      ,RM=  .400000010    ,RM=  2.00000000    ,CONV=  .1000000360E-05,AI=  .200000002    ,A2=  .149999975    ,A3=
  3.00999999      ,RN=  9000000.00    ,XIDELV=  .429999995    ,CIR=  0.            ,CDCURR=  0.            ,RDEL=  .250000000
RDELFN=  .125000000    ,SP=  .400000006E-02,XSEP=  .439999998    ,XCP0=  .199999988    ,CP0=  .399999976    ,RNSN=  .479000020
RLSEP=  .000000000    ,SPC=  .000000000    ,RLSDLY=  .429999995    ,RLAS=  1.00000000    ,NADUS=  .100000000E-01
$END
$LIND
IMAS=          13,JMAS=          7,IBASE=          800,INV=          0,MITER=          1000,RMALP=          2,ITACT=          1,ISKP2=
          0,ISKP3=          0,ISKP4=          0,ITERP=          0,IREAD=          0,LP=          1000,IMASS=          1,ILAM=
          1,IPRT1=          0,IPRT2=          0,KSEP=          1
$END

                         H-V GRID SYSTEM

   2 -0 14108E+01    3 -0 48000E+00    4 -0 37058E+00    5 -0 24858E+00    6 -0 12478E+00    7  0  0
   8  0 12478E+00    9  0 24858E+00   10  0 37058E+00   11  0 48000E+00   12  0 14108E+01
   2 -0 42818E+00    3 -0 14308E+00    4 -0 23038E-07    5  0 14308E+00    6  0 42818E+00

                    AIRFOIL COORDINATES
     X          YU          YL    UPPER SLOPE   LOWER SLOPE
 -0 00000    0 01706   -0 01706    0 81058   -0 81058
 -0 37058    0 05112   -0 05112    0 12838   -0 12838
 -0 24852    0 05846   -0 05846    0 02438   -0 02438
 -0 12478    0 05855   -0 05855   -0 02838    0 02838
  0 0        0 05284   -0 05284   -0 05318    0 05318
  0 12478    0 04385   -0 04385   -0 05815    0 05815
  0 24852    0 03178   -0 03178   -0 10283    0 10383
  0 37058    0 01808   -0 01808   -0 12032    0 12032
  0 48000    0 00265   -0 00265   -0 13858    0 13858
ITERATION  10 CIR =  0 20712 DPM =  0 01805503 AT 12  3 MSP =    0 DELTAV BR TWITE  =  0 9027 SEP AT 3 =    0 800
ITERATION  20 CIR =  0 42348 DPM =  0 01387038 AT 12  3 MSP =    0 DELTAV CR TWITE  =    0027 SEP AT 3 =    0 800
ITERATION  30 CIR =  0 53834 DPM =  0 01065498 AT 10  3 MSP =    0 DELTAV BR TWITE  =  0 0027 SEP AT 3 =    0 800
ITERATION  40 CIR =  0 61811 DPM =  0 00788702 AT  8  3 MSP =    0 DELTAV CR TWITE  =  0 0027 SEP AT 3 =    0 800
ITERATION  50 CIR =  0 67323 DPM =  0 00598323 AT  8  3 MSP =    2 DELTAV BR TWITE  =  0 0027 SEP AT 3 =    0 800

 CP BY CENTRAL DIFFERENCES
X          CPU          CPL
     0 450        7 801        1 027
     1 371        7 288        0 171
     0 248          116        0 031
       25        1 684        0 033
     0 0         -0 899        0 045
     0 125       -0 483        0 071
     0 249       -0 309        0 107
     0 371       -0 102        0 171
     0 450        0 828        0 874
X          YU          YL          SLU          SLL
 -0 00000    0 01706   -0 01706    0 81058   -0 81058
 -0 37058    0 05112   -0 05112    0 12838   -0 12838
 -0 24852    0 05846   -0 05846    0 02438   -0 02438
 -0 12478    0 05855   -0 05855   -0 02838    0 02838
  0 0        0 05284   -0 05284   -0 05318    0 05318

  0 12478    0 04385   -0 04385   -0 05815    0 05815
  0 24852    0 03178   -0 03178   -0 10383    0 10383
  0 37058    0 01808   -0 01808   -0 12032    0 12032
  0 48000    0 00265    0 00265   -0 13858    0 13858

                              MACH CHART IN COMPUTATIONAL                    PLANE-FREE STREAM FROM TOP

  I=3,12 TOP TO BOTTOM

  J= 2, 8 LEFT TO RIGHT

 56 48 48 51 53
 26 15  0161 44
 43 43  0102 55
 45 46  0 77 57
 45 47  0 71 56
 45 47  0 66 51
 45 47  0 61 54
 45 46    57 51
 41 41    2 53
  1 33  1  1 50
  0 44 47 48 48

                    NORMAL FORCE COEFFICIENT CN BY INTEGRATION =      1 2101

                    WAVE CD =    0 103894
                    THEORETICALLY ZERO FOR SUBCRITICAL CASES
```

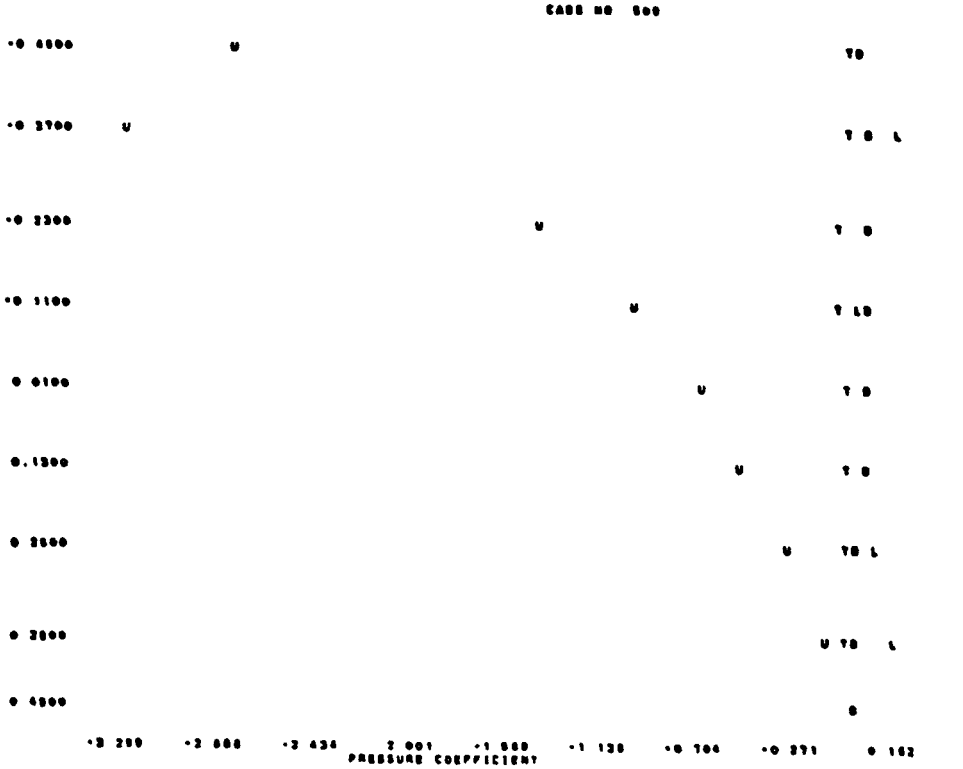


```
TEST CASE, NACA 0012, MACH 0 8  RN 9 MILLION  ALPHA 0 25 DEG

                    CASE NUMBER   509

          MACH NO  IS 0 80ANGLE OF ATTACK IS  0 250 DEGREES

                   INVISCID ANALYSIS CASE
                   WITH LAMINAR TURBULENT VISCOUS INTERACTION
                   AND MASSIVE SEPARATION
                   AND VARIABLE PRESSURE IN SEPARATED REGION
&PINP
MI=  800000001     WI=  1 00000001     XI=  500000000     X2=  10000 0000     ALP=  181643875     EPS=  0             EPSS=
  1 00000000    ,XS=  480000010    ,S4=  2 00000000     CONV=  1000000348 05 AI=  248888882    ,A2=  148888878    ,A3=
  2 88888889    RN=  8000000 00     RIBOLY=  4 438888888     CIR=  673234781     CDCORR=  0          ,RDEL=  280000000
BOELPN=  135000000     SP=  4000000888 02 XSEP=  438888888     ACP8=  188888888     CPB=  388888878     RMON=  478000028
XLEEP=  800000000     XPC=  800000000     XLEOLY=  438888888     RLAR=  1 00000000     RADUS=  1880000888E-01
&ENC
&IINP
IMAX=          25 JMAX=          13 IKASE=          800 INV=          0 MITER=          800 NHALF=          2 ITACT=          1 ISKP2=
          0 ISKP3=          0 ISKP4=          0,ITERP=          0 IREAD=          0 LP=          1000 IMASS=          1 ILAM=
          1 IPRT1=          0,IPRT2=          0 KEEP=          1
&END

                   X-Y GRID SYSTEM

   2  +0 38728+01     3  -0 14108+01     4   0 64718+00     5   0 68008+00     6  +0 43078+00     7   0 37068+00
   8   0 30588+00     9   0 24888+00    10   0 18868+00    11   0 12478+00    12   0 6240E 01    13   0 0
  14   0 6240E 01    15   0 12478+00    16   0 18888+00    17   0 24858+00    18   0 30988+00    19   0 37068+00
  20   0 43078+00    21   0 48008+00    22   0 64718+00    23   0 14108+01    24   0 38728+01
   2   0 81818+00     3   0 42818+00     4   0 24808+00     5   0 14208+00     6   0 88928 01     7  -0 82138-07
   8   0 88928 01     9   0 14208+00    10   0 24808+00    11   0 42818+00    12   0 81818+00
```

AIRFOIL COORDINATES

X	YU	YL	UPPER SLOPE	LOWER SLOPE
.0 .00000	.0 .01704	.0 .01704	.0 .01058	.0 .01058
.0 .03057	.0 .04070	.0 .04070	.0 .21576	.0 .23576
.0 .37058	.0 .05112	.0 .05112	.0 .12539	.0 .12539
.0 .30057	.0 .05577	.0 .05577	.0 .05521	.0 .05521
.0 .24057	.0 .05868	.0 .05868	.0 .02436	.0 .02436
.0 .18077	.0 .05888	.0 .05888	.0 .00588	.0 .00588
.0 .12078	.0 .05885	.0 .05885	.0 .02838	.0 .02838
.0 .08240	.0 .05862	.0 .05862	.0 .04802	.0 .04802
.0 .0	.0 .05284	.0 .05284	.0 .08316	.0 .08316
.0 .03240	.0 .04850	.0 .04850	.0 .07958	.0 .07958
.0 .12078	.0 .04358	.0 .04358	.0 .08816	.0 .08816
.0 .18077	.0 .03781	.0 .03781	.0 .09541	.0 .09541
.0 .24057	.0 .03178	.0 .03178	.0 .10303	.0 .10303
.0 .30057	.0 .02614	.0 .02614	.0 .11200	.0 .11200
.0 .37058	.0 .01988	.0 .01988	.0 .12033	.0 .12033
.0 .43057	.0 .01585	.0 .01585	.0 .12803	.0 .12803
.0 .48000	.0 .00285	.0 .00285	.0 .13500	.0 .13500

ITERATION 10 CIR = .0 .88974 DPM = .0 .000186711 AT 6 .6 NSSP = 3 DELTAY OR YUITE = .0 .0027 SEP AT X = .0 .500

ITERATION 20 CIR = .0 .88972 DPM = .0 .000085203 AT 6 .12 NSSP = 3 DELTAY OR YUITE = .0 .0027 SEP AT X = .0 .500

ITERATION 30 CIR = .0 .88934 DPM = .0 .000041888 AT 16 .6 NSSP = 3 DELTAY OR YUITE = .0 .0027 SEP AT X = .0 .500

ITERATION 40 CIR = .0 .87188 DPM = .0 .000038648 AT 17 .6 NSSP = 3 DELTAY OR YUITE = .0 .0027 SEP AT X = .0 .500

ITERATION 50 CIR = .0 .87468 DPM = .0 .000032288 AT 17 .6 NSSP = 3 DELTAY OR YUITE = .0 .0027 SEP AT X = .0 .500

USTCK LT ZERO

ITERATION 60 CIR = .0 .83232 DPM = .0 .000000038 AT 24 .6 NSSP = 4 DELTAY OR YUITE = .0 .0276 SEP AT X = .0 .431

USTCK LT ZERO

ITERATION 70 CIR = .0 .81867 DPM = .0 .000162883 AT 24 .6 NSSP = 4 DELTAY OR YUITE = .0 .0247 SEP AT X = .0 .371

ITERATION 80 CIR = .0 .80273 DPM = .0 .000120803 AT 24 .6 NSSP = 4 DELTAY OR YUITE = .0 .0175 SEP AT X = .0 .371

ITERATION 90 CIR = .0 .80064 DPM = .0 .000088838 AT 24 .6 NSSP = 3 DELTAY OR YUITE = .0 .0203 SEP AT X = .0 .371

ITERATION 100 CIR = .0 .80032 DPM = .0 .000051768 AT 24 .6 NSSP = 3 DELTAY OR YUITE = .0 .0188 SEP AT X = .0 .371

ITERATION 110 CIR = .0 .87111 DPM = .0 .000052388 AT 24 .6 NSSP = 3 DELTAY OR YUITE = .0 .0204 SEP AT X = .0 .371

ITERATION 120 CIR = .0 .80383 DPM = .0 .000078038 AT 23 .6 NSSP = 3 DELTAY OR YUITE = .0 .0208 SEP AT X = .0 .371

ITERATION 130 CIR = .0 .80863 DPM = .0 .000078238 AT 24 .6 NSSP = 3 DELTAY OR YUITE = .0 .0214 SEP AT X = .0 .371

ITERATION 140 CIR = .0 .80810 DPM = .0 .000081168 AT 23 .6 NSSP = 3 DELTAY OR YUITE = .0 .0220 SEP AT X = .0 .371

ITERATION 150 CIR = .0 .80324 DPM = .0 .000080018 AT 23 .6 NSSP = 3 DELTAY OR YUITE = .0 .0220 SEP AT X = .0 .371

ITERATION 160 CIR = .0 .83786 DPM = .0 .000082243 AT 23 .6 NSSP = 3 DELTAY OR YUITE = .0 .0223 SEP AT X = .0 .371

ITERATION 170 CIR = .0 .83318 DPM = .0 .000081878 AT 23 .6 NSSP = 3 DELTAY OR YUITE = .0 .0230 SEP AT X = .0 .371

ITERATION 180 CIR = .0 .82882 DPM = .0 .000080881 AT 23 .6 NSSP = 3 DELTAY OR YUITE = .0 .0233 SEP AT X = .0 .371

ITERATION 190 CIR = .0 .82484 DPM = .0 .000083188 AT 23 .6 NSSP = 3 DELTAY OR YUITE = .0 .0283 SEP AT X = .0 .371

ITERATION 200 CIR = .0 .82120 DPM = .0 .000080188 AT 23 .6 NSSP = 3 DELTAY OR YUITE = .0 .0288 SEP AT X = .0 .371

ITERATION 210 CIR = .0 .81786 DPM = .0 .000079138 AT 23 .6 NSSP = 3 DELTAY OR YUITE = .0 .0286 SEP AT X = .0 .371

ITERATION 220 CIR = .0 .81478 DPM = .0 .000078181 AT 23 .6 NSSP = 3 DELTAY OR YUITE = .0 .0271 SEP AT X = .0 .371

ITERATION 230 CIR = .0 .81188 DPM = .0 .000076426 AT 23 .6 NSSP = 3 DELTAY OR YUITE = .0 .0276 SEP AT X = .0 .371

ITERATION 240 CIR = .0 .80923 DPM = .0 .000078188 AT 23 .6 NSSP = 3 DELTAY OR YUITE = .0 .0288 SEP AT X = .0 .371

ITERATION 250 CIR = .0 .80678 DPM = .0 .000077116 AT 23 .6 NSSP = 3 DELTAY OR YUITE = .0 .0283 SEP AT X = .0 .371

ITERATION 260 CIR = .0 .80443 DPM = .0 .000075328 AT 23 .6 NSSP = 3 DELTAY OR YUITE = .0 .0288 SEP AT X = .0 .371

ITERATION 270 CIR = .0 .80224 DPM = .0 .000073286 AT 23 .6 NSSP = 3 DELTAY OR YUITE = .0 .0300 SEP AT X = .0 .371

ITERATION 280 CIR = .0 .80020 DPM = .0 .000071488 AT 23 .6 NSSP = 3 DELTAY OR YUITE = .0 .0304 SEP AT X = .0 .371

ITERATION 290 CIR = .0 .49827 DPM = .0 .000070805 AT 23 .6 NSSP = 3 DELTAY OR YUITE = .0 .0308 SEP AT X = .0 .371

ITERATION 300 CIR = .0 .49644 DPM = .0 .000178868 AT 23 .6 NSSP = 3 DELTAY OR YUITE = .0 .0313 SEP AT X = .0 .371

ITERATION 310 CIR = .0 .49491 DPM = .0 .000177887 AT 23 .6 NSSP = 3 DELTAY OR YUITE = .0 .0317 SEP AT X = .0 .371

ITERATION 320 CIR = .0 .49307 DPM = .0 .000174488 AT 23 .6 NSSP = 3 DELTAY OR YUITE = .0 .0321 SEP AT X = .0 .371

ITERATION 330 CIR = .0 .49180 DPM = .0 .000168388 AT 22 .6 NSSP = 3 DELTAY OR YUITE = .0 .0325 SEP AT X = .0 .371

ITERATION 340 CIR = .0 .49002 DPM = .0 .000165988 AT 23 .6 NSSP = 3 DELTAY OR YUITE = .0 .0328 SEP AT X = .0 .371

ITERATION 350 CIR = .0 .48880 DPM = .0 .000164883 AT 24 .6 NSSP = 3 DELTAY OR YUITE = .0 .0333 SEP AT X = .0 .371

ITERATION 360 CIR = .0 .48724 DPM = .0 .000123483 AT 24 .6 NSSP = 3 DELTAY OR YUITE = .0 .0335 SEP AT X = .0 .371

ITERATION 370 CIR = .0 .48586 DPM = .0 .000160881 AT 24 .6 NSSP = 3 DELTAY OR YUITE = .0 .0338 SEP AT X = .0 .371

ITERATION 380 CIR = .0 .48471 DPM = .0 .000127436 AT 23 .6 NSSP = 3 DELTAY OR YUITE = .0 .0341 SEP AT X = .0 .371

ITERATION 390 CIR = .0 .48362 DPM = .0 .000111674 AT 23 .6 NSSP = 3 DELTAY OR YUITE = .0 .0344 SEP AT X = .0 .371

ITERATION 400 CIR = .0 .48238 DPM = .0 .000111170 AT 23 .6 NSSP = 3 DELTAY OR YUITE = .0 .0347 SEP AT X = .0 .371

ITERATION 410 CIR = .0 .48128 DPM = .0 .000108497 AT 23 .6 NSSP = 3 DELTAY OR YUITE = .0 .0349 SEP AT X = .0 .371

ITERATION 420 CIR = .0 .48026 DPM = .0 .000103867 AT 24 .6 NSSP = 3 DELTAY OR YUITE = .0 .0352 SEP AT X = .0 .371

ITERATION 430 CIR = .0 .47926 DPM = .0 .000102308 AT 24 .6 NSSP = 3 DELTAY OR YUITE = .0 .0354 SEP AT X = .0 .371

ITERATION 440 CIR = .0 .47826 DPM = .0 .000114488 AT 24 .6 NSSP = 3 DELTAY OR YUITE = .0 .0358 SEP AT X = .0 .371

ITERATION 450 CIR = .0 .47735 DPM = .0 .000098288 AT 23 .6 NSSP = 3 DELTAY OR YUITE = .0 .0359 SEP AT X = .0 .371

ITERATION 460 CIR = .0 .47648 DPM = .0 .000098188 AT 24 .6 NSSP = 3 DELTAY OR YUITE = .0 .0361 SEP AT X = .0 .371

ITERATION 470 CIR = .0 .47580 DPM = .0 .000084008 AT 23 .6 NSSP = 3 DELTAY OR YUITE = .0 .0363 SEP AT X = .0 .371

ITERATION 480 CIR = .0 .47497 DPM = .0 .000091883 AT 23 .6 NSSP = 3 DELTAY OR YUITE = .0 .0365 SEP AT X = .0 .371

ITERATION 490 CIR = .0 .47388 DPM = .0 .000082214 AT 23 .6 NSSP = 3 DELTAY OR YUITE = .0 .0367 SEP AT X = .0 .371

ITERATION 500 CIR = .0 .47322 DPM = .0 .000085228 AT 24 .6 NSSP = 3 DELTAY OR YUITE = .0 .0369 SEP AT X = .0 .371

ITERATION 510 CIR = .0 .47248 DPM = .0 .000071122 AT 24 .6 NSSP = 3 DELTAY OR YUITE = .0 .0370 SEP AT X = .0 .371

ITERATION 520 CIR = .0 .47178 DPM = .0 .000073118 AT 24 .6 NSSP = 3 DELTAY OR YUITE = .0 .0372 SEP AT X = .0 .371

ITERATION 530 CIR = .0 .47111 DPM = .0 .000068851 AT 23 .6 NSSP = 3 DELTAY OR YUITE = .0 .0373 SEP AT X = .0 .371

ITERATION 540 CIR = .0 .47048 DPM = .0 .000068868 AT 23 .6 NSSP = 3 DELTAY OR YUITE = .0 .0375 SEP AT X = .0 .371

ITERATION 550 CIR = .0 .46983 DPM = .0 .000065328 AT 23 .6 NSSP = 3 DELTAY OR YUITE = .0 .0376 SEP AT X = .0 .371

ITERATION 560 CIR = .0 .46923 DPM = .0 .000061567 AT 23 .6 NSSP = 3 DELTAY OR YUITE = .0 .0378 SEP AT X = .0 .371

ITERATION 570 CIR = .0 .46868 DPM = .0 .000058178 AT 24 .6 NSSP = 3 DELTAY OR YUITE = .0 .0378 SEP AT X = .0 .371

ITERATION 580 CIR = .0 .46810 DPM = .0 .000073678 AT 24 .6 NSSP = 3 DELTAY OR YUITE = .0 .0381 SEP AT X = .0 .371

ITERATION 590 CIR = .0 .46767 DPM = .0 .000070231 AT 24 .6 NSSP = 3 DELTAY OR YUITE = .0 .0383 SEP AT X = .0 .371

ITERATION 600 CIR = .0 .46708 DPM = .0 .000064908 AT 24 .6 NSSP = 3 DELTAY OR YUITE = .0 .0383 SEP AT X = .0 .371

ITERATION 610 CIR = .0 .46688 DPM = .0 .000055778 AT 24 .6 NSSP = 3 DELTAY OR YUITE = .0 .0384 SEP AT X = .0 .371

ITERATION 620 CIR = .0 .46608 DPM = .0 .000064888 AT 23 .6 NSSP = 3 DELTAY OR YUITE = .0 .0385 SEP AT X = .0 .371

ITERATION 630 CIR = .0 .46563 DPM = .0 .000048971 AT 23 .6 NSSP = 3 DELTAY OR YUITE = .0 .0385 SEP AT X = .0 .371

ITERATION 640 CIR = .0 .46518 DPM = .0 .000041107 AT 22 .6 NSSP = 3 DELTAY OR YUITE = .0 .0387 SEP AT X = .0 .371

ITERATION 650 CIR = .0 .46477 DPM = .0 .000042288 AT 2 .6 NSSP = 3 DELTAY OR YUITE = .0 .0388 SEP AT X = .0 .371

ITERATION 660 CIR = .0 .46437 DPM = .0 .000033988 AT 23 .6 NSSP = 3 DELTAY OR YUITE = .0 .0388 SEP AT X = .0 .371

ITERATION 670 CIR = .0 .46398 DPM = .0 .000044111 AT 24 .6 NSSP = 3 DELTAY OR YUITE = .0 .0388 SEP AT X = .0 .371

ITERATION 680 CIR = .0 .46381 DPM = .0 .000039934 AT 23 .6 NSSP = 3 DELTAY OR YUITE = .0 .0391 SEP AT X = .0 .371

ITERATION 690 CIR = .0 .46326 DPM = .0 .000047188 AT 24 .6 NSSP = 3 DELTAY OR YUITE = .0 .0392 SEP AT X = .0 .371

ITERATION 700 CIR = .0 .46281 DPM = .0 .000043408 AT 24 .6 NSSP = 3 DELTAY OR YUITE = .0 .0393 SEP AT X = .0 .371

ITERATION 710 CIR = .0 .46256 DPM = .0 .000032588 AT 23 .6 NSSP = 3 DELTAY OR YUITE = .0 .0393 SEP AT X = .0 .371

ITERATION 720 CIR = .0 .46227 DPM = .0 .000033988 AT 23 .6 NSSP = 3 DELTAY OR YUITE = .0 .0394 SEP AT X = .0 .371

ITERATION 730 CIR = .0 .46188 DPM = .0 .000031888 AT 23 .6 NSSP = 3 DELTAY OR YUITE = .0 .0395 SEP AT X = .0 .371

ITERATION 740 CIR = .0 .46167 DPM = .0 .000027748 AT 30 .6 NSSP = 3 DELTAY OR YUITE = .0 .0395 SEP AT X = .0 .371

ITERATION 750 CIR = .0 .46138 DPM = .0 .000044858 AT 24 .6 NSSP = 3 DELTAY OR YUITE = .0 .0396 SEP AT X = .0 .371

ITERATION 760 CIR = .0 .46112 DPM = .0 .000044088 AT 24 .6 NSSP = 3 DELTAY OR YUITE = .0 .0397 SEP AT X = .0 .371

ITERATION 770 CIR = .0 .46086 DPM = .0 .000027718 AT 3 .6 NSSP = 3 DELTAY OR YUITE = .0 .0397 SEP AT X = .0 .371

ITERATION 780 CIR = .0 .46062 DPM = .0 .000021488 AT 23 .6 NSSP = 3 DELTAY OR YUITE = .0 .0398 SEP AT X = .0 .371

ITERATION 790 CIR = .0 .46038 DPM = .0 .000023988 AT 23 .6 NSSP = 3 DELTAY OR YUITE = .0 .0399 SEP AT X = .0 .371

ITERATION 800 CIR = .0 .46015 DPM = .0 .000022891 AT 22 .6 NSSP = 3 DELTAY OR YUITE = .0 .0399 SEP AT X = .0 .371

ORIGINAL PAGE IS
OF POOR QUALITY

BOUNDARY LAYER ANALYSIS FOR REYNOLDS NUMBER OF 0.8008+07

X	YUDRIC	DU	SLU	YLDRIC	DL	SLL
+0 49000	0 01704	0 0	0 01058	+0 01704	0 0	+0 01058
+0 43057	0 04070	0 00016	0 10721	+0 04070	0 00016	+0 10552
+0 37058	0 05112	0 00038	0 13870	+0 05112	0 00038	+0 13575
+0 30882	0 05877	0 00070	0 05847	+0 05877	0 00032	+0 05225
+0 24852	0 05845	0 00110	0 03171	+0 05845	0 00038	+0 02870
+0 18677	0 05888	0 00151	0 00057	+0 05888	0 00036	0 00642
+0 12670	0 05885	0 00184	+0 02218	+0 05886	0 00036	0 02866
+0 06340	0 05842	0 00240	0 04025	0 05842	0 00028	0 04738
0 0	0 05284	0 00281	+0 05441	+0 05284	0 00042	0 05248
0 06240	0 04886	0 00268	+0 05845	+0 04886	0 00041	0 07498
0 12670	0 04305	0 00418	+0 07275	+0 04305	0 00050	0 08858
0 18677	0 03701	0 00510	+0 07886	+0 03701	0 00053	0 08463
0 24852	0 03178	0 00584	+0 06235	+0 03176	0 00056	0 10300
0 30882	0 02614	0 01062	+0 02784	+0 02614	0 00055	0 11012
0 37058	0 01806	0 01722	0 00131	+0 01806	0 00063	0 11854
0 43057	0 01059	0 02545	0 03783	+0 01059	0 00108	0 12648
0 49000	0 00285	0 03647	0 08903	+0 00285	0 00136	0 13612

CP BY CENTRAL DIFFERENCES

X	CPU	CPL
+0 490	-2 723	1 040
+0 431	-2 867	0 881
+0 371	-1 718	0 350
+0 310	-1 383	0 228
+0 248	-1 078	0 180
+0 187	-0 881	0 113
+0 125	-0 717	0 081
+0 063	-0 577	0 060
0 0	-0 464	0 047
0 063	-0 360	0 038
0 125	-0 285	0 033
0 187	-0 112	0 030
0 248	0 002	0 030
0 310	0 076	0 032
0 371	0 107	0 035
0 431	0 157	0 043
0 490	0 198	0 116

X	YU	YL	SLU	SLL
0 49000	0 01703	-0 01703	0 01058	+0 01058
+0 43057	0 04088	-0 04088	0 10721	+0 10552
+0 37058	0 05151	-0 05130	0 13870	+0 13575
+0 30882	0 05744	-0 05899	0 05847	+0 05225
0 24852	0 05854	-0 05971	0 03171	+0 02870
+0 18677	0 05146	-0 05028	0 00057	0 00642
+0 12670	0 05915	+0 05920	-0 02218	0 02866
+0 06340	0 05882	+0 05881	+0 04025	0 04738
0 0	0 05886	+0 05336	+0 05441	0 05248
0 06240	0 05209	+0 04805	+0 05845	0 07498
0 12670	0 04776	0 04605	+0 07275	0 08858
0 18677	0 04303	+0 03845	+0 07886	0 08463
0 24852	0 03881	0 03234	0 06235	0 10300
0 30882	0 03177	+0 03800	0 02784	0 11012
0 37058	0 03488	+0 01881	0 00131	0 11854
0 43057	0 03613	+0 01189	0 03783	0 12648
0 49000	0 03892	0 00402	0 08903	0 13612

MACH CHART IN COMPUTATIONAL PLANE FROM STORAGE FROM TAP

I=3,24 TOP TO BOTTOM

J= 2,13 LEFT TO RIGHT

```
80 80 80 80 80 80 80 80 80 80 80 80
48 48 48 48 48 48 48 80 80 81 81 81
48 48 44 43 43 47 82 85 86 85 84 84
43 38 31 24 14  0101 87 79 70 69 69
48 43 38 36 33  0105 84 72 63 86 86
48 43 40 38 38  0 86 78 71 63 86 86
48 43 42 42 43  0 81 75 69 63 86 86
48 44 43 44 46  0 76 72 67 62 86 86
48 48 48 48 48  0 71 83 85 81 85 85
48 48 48 48 47  0 87 85 83 80 86 86
48 48 48 47 48  0 84 83 81 83 86 86
47 48 47 47 48  0 81 80 80 86 86 86
47 47 47 48 48  0 86 86 87 86 84 84
47 47 47 48 48  0 85 85 85 85 84 84
47 47 48 48 48  0 83 83 84 84 84 84
47 47 48 48 48  0 80 81 82 83 83 83
47 47 48 48 48  0 48 80 81 82 83 83
47 48 48 48 48  0 47 49 80 82 83 83
47 48 48 48 48  0 47 48 80 81 82 83
47 47 47 47 47  0 46 48 80 82 84 84
48 48 48 48 48 48 48 48 80 80 81 81
48 48 48 48 48 48 48 48 80 80 80 80
48 48 48 48 48 48 48 48 48 48 48 48
```

NORMAL FORCE COEFFICIENT CN BY INTEGRATION = 0.8487

WAVE CD = 0.087634
THEORETICALLY ZERO FOR SUBCRITICAL CASES

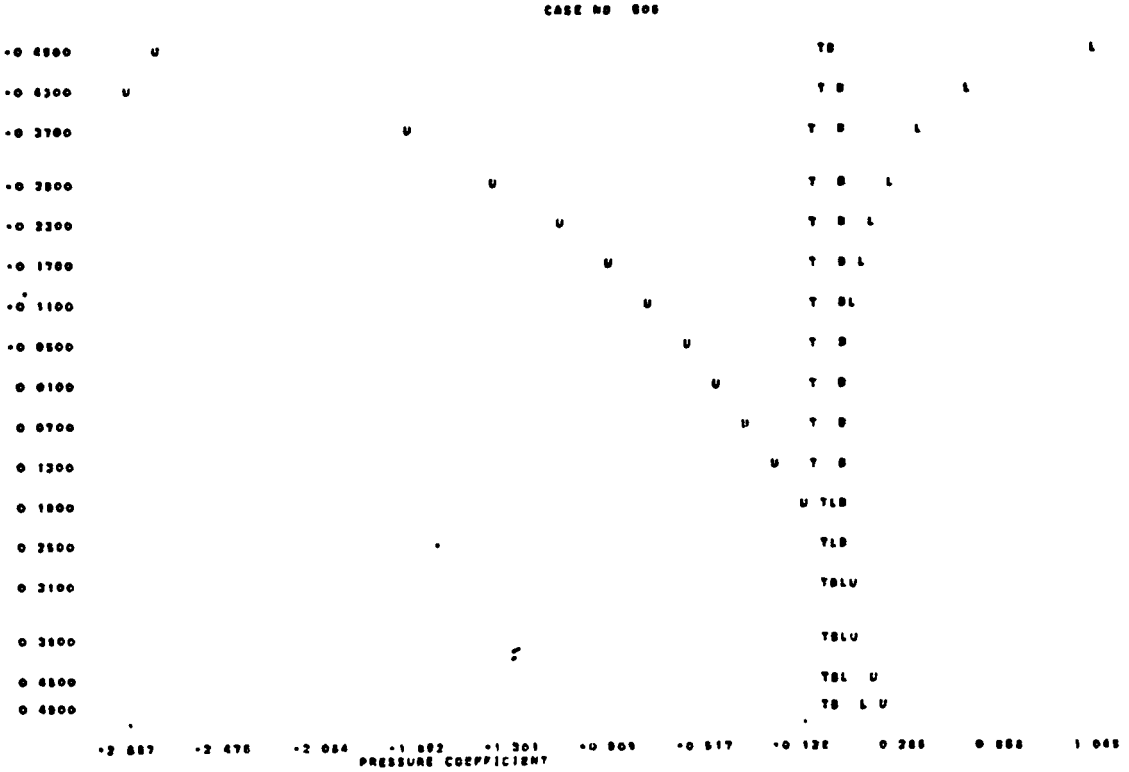


```
EST CASE  NACA 0012, MACH 0 8, RN 6 MILLION  ALPHA 0 25 DEG
                        CASE NUMBER   809
              MACH NO  IS 0 8010ANGLE OF ATTACK IS   0 250 DEGREES
                       INVISCID ANALYSIS CASE
                       WITH LAMINAR TURBULENT VISCOUS INTERACTION
                       AND MASSIVE SEPARATION
                       AND VARIABLE PRESSURE IN SEPARATED REGION
&FINP
M=   8000000047     ,W=  1 00000001     R1=   368917044     X2=   000000000     ALP=   161442878     EPS=                EPSS=
   1 00000000     R4=   480000010     S0=  2 00000000     CONV=  1000000042-05 A1=   245888852     A2=   4E9817875     ,A3=
   3 88888888     R4=  8000000 00     RIBDLY=  - 438888886     CIR=   480148825     CDCDRR=   0          AOEL=   2880000000
&DELPH=   125000000     ,EP=   400000008E 02,EBEP=   438888888     RCP8=   188888888     CP8=   38888887     M3N=   47C0000021
&LEEP=   800000000     ,RPC=   80C000000     ,RLBDLY=  - 438888888     RLAX=  1 00000000     ,RADUS=   1880000008E 01
&END
&LINP
IMAX=          88 JMAX=          25 IRASE=         800 INV=           0 MITER=         400 MNALP=           2 ITACT=           1 IBKP
          0,ISKP3=           0 ISKP4=           0 ITERP=           0,IREAD=           0,LP=        1000 IMASS=           1,ELAM=
          1 IP8T1=           0,IP8T2=           0 KSEP=            1
&END
```

ORIGINAL PAGE IS
OF POOR QUALITY

X-Y GRID SYSTEM

2	-0 .60270E+01	3	-0 .38720E+01	4	-0 .32700E+01	5	-0 .14100E+01	6	-0 .81150E+00	7	-0 .84710E+00
8	-0 .83170E+00	9	-0 .69000E+00	10	-0 .48040E+00	11	-0 .43070E+00	12	-0 .40070E+00	13	-0 .37050E+00
14	-0 .34030E+00	15	-0 .30990E+00	16	0 .27020E+00	17	-0 .24000E+00	18	-0 .21770E+00	19	-0 .18580E+00
20	-0 .15580E+00	21	-0 .12470E+00	22	-0 .03570E-01	23	-0 .02400E-01	24	-0 .31210E-01	25	0 .0
26	0 .31210E-01	27	0 .0240E-01	28	0 .03570E-01	29	0 .12470E+00	30	0 .15580E+00	31	0 .18580E+00
32	0 .21770E+00	33	0 .24000E+00	34	0 .27020E+00	35	0 .30990E+00	36	0 .34030E+00	37	0 .37050E+00
38	0 .40070E+00	39	0 .43070E+00	40	0 .48040E+00	41	0 .69000E+00	42	0 .83170E+00	43	0 .84710E+00
44	0 .81150E+00	45	0 .14100E+01	46	0 .32700E+01	47	0 .38720E+01	48	0 .60270E+01		
1	-0 .18000E+01	2	-0 .81610E+00	4	-0 .50300E+00	5	-0 .42810E+00	6	-0 .32000E+00	7	-0 .24000E+00
8	-0 .18000E+00	9	-0 .14200E+00	10	-0 .10100E+00	11	-0 .85020E-01	12	-0 .32330E-01	13	-0 .02130E-01
14	0 .32330E-01	15	0 .8502E-01	16	0 .10100E+00	17	0 .14200E+00	18	0 .18000E+00	19	0 .24000E+00
20	0 .32000E+00	21	0 .42810E+00	22	0 .50300E+00	23	0 .81610E+00	24	0 .18000E+01		

AIRFOIL COORDINATES

X	YU	YL	UPPER SLOPE	LOWER SLOPE
-0 .60000	0 .01706	-0 .01706	0 .81058	-0 .81058
-0 .48044	0 .03212	-0 .03212	0 .38634	-0 .38634
-0 .43087	0 .04070	-0 .04070	0 .18721	-0 .18882
-0 .40072	0 .04830	-0 .04808	0 .18846	-0 .18858
-0 .37058	0 .05191	-0 .05130	0 .13838	-0 .13878
-0 .34028	0 .05448	-0 .05418	0 .10408	-0 .09880
-0 .30982	0 .05748	-0 .05888	0 .08847	-0 .08328
-0 .27823	0 .05801	-0 .05835	0 .05009	-0 .04852
-0 .24852	0 .05856	-0 .05871	0 .03171	-0 .03578
-0 .21788	0 .05101	-0 .05800	0 .01818	-0 .01018
-0 .18877	0 .05118	-0 .04038	0 .00067	0 .00842
-0 .15877	0 .05116	-0 .05874	-0 .01074	0 .01704
-0 .12470	0 .05078	-0 .05838	-0 .02216	0 .02888
-0 .09367	0 .05861	-0 .05800	-0 .03128	0 .03803
-0 .06240	0 .05867	-0 .05861	-0 .04028	0 .04738
-0 .03121	0 .05726	-0 .05808	-0 .04726	0 .05484
0 .0	0 .05885	-0 .05328	-0 .05448	0 .05260
0 .03121	0 .05387	-0 .05121	-0 .05888	0 .05874
0 .06240	0 .05209	-0 .04806	-0 .05548	0 .07888
0 .09367	0 .04882	-0 .04858	-0 .06862	0 .08028
0 .12470	0 .04774	-0 .04405	-0 .07378	0 .08886
0 .15877	0 .04538	-0 .04125	-0 .07838	0 .09020
0 .18877	0 .04303	-0 .03846	-0 .07886	0 .09483
0 .21788	0 .04082	-0 .03538	-0 .08858	0 .09851
0 .24852	0 .03881	-0 .03234	0 .08235	0 .10306
0 .27823	0 .03718	0 .02907	-0 .04484	0 .10856
0 .30982	0 .03577	-0 .02560	-0 .02784	0 .11012
0 .34028	0 .03537	-0 .02238	-0 .01311	0 .11333
0 .37058	0 .03488	-0 .01881	0 .00131	0 .11854
0 .40072	0 .03598	-0 .01538	0 .01881	0 .12051
0 .43087	0 .03613	-0 .01188	0 .03782	0 .12448
0 .48044	0 .03803	-0 .00788	0 .05343	0 .12930
0 .48000	0 .03892	-0 .00402	0 .05803	0 .13412

ITERATION	10	CIR	=	0 .46257	DPM	=	0 .00058022	AT	38	2	NSSP	=	5	DELTAY OR YUITE	=	0 .0388	SEP AT X	=	0 .371
ITERATION	20	CIR	=	0 .46546	DPM	=	0 .00018893	AT	47	11	NSSP	=	5	DELTAY OR YUITE	=	0 .0388	SEP AT X	=	0 .371
ITERATION	30	CIR	=	0 .46677	DPM	=	0 .00012100	AT	37	2	NSSP	=	5	DELTAY OR YUITE	=	0 .0388	SEP AT X	=	0 .371
ITERATION	40	CIR	=	0 .46780	DPM	=	0 .00010454	AT	47	10	NSSP	=	5	DELTAY OR YUITE	=	0 .0388	SEP AT X	=	0 .371
ITERATION	50	CIR	=	0 .46885	DPM	=	0 .00014063	AT	47	12	NSSP	=	5	DELTAY OR YUITE	=	0 .0389	SEP AT X	=	0 .371
ITERATION	60	CIR	=	0 .46880	DPM	=	0 .00006886	AT	38	15	NSSP	=	5	DELTAY OR YUITE	=	0 .0412	SEP AT X	=	0 .371
ITERATION	70	CIR	=	0 .46868	DPM	=	0 .00010317	AT	48	11	NSSP	=	5	DELTAY OR YUITE	=	0 .0451	SEP AT X	=	0 .371
ITERATION	80	CIR	=	0 .46868	DPM	=	0 .00006588	AT	2	14	NSSP	=	5	DELTAY OR YUITE	=	0 .0446	SEP AT X	=	0 .371
ITERATION	90	CIR	=	0 .46834	DPM	=	0 .00005734	AT	46	12	NSSP	=	5	DELTAY OR YUITE	=	0 .0446	SEP AT X	=	0 .371
ITERATION	100	CIR	=	0 .46885	DPM	=	0 .00018582	AT	48	8	NSSP	=	5	DELTAY OR YUITE	=	0 .0445	SEP AT X	=	0 .371
ITERATION	110	CIR	=	0 .47002	DPM	=	0 .00010782	AT	48	13	NSSP	=	5	DELTAY OR YUITE	=	0 .0444	SEP AT X	=	0 .371
ITERATION	120	CIR	=	0 .47040	DPM	=	0 .00008781	AT	47	12	NSSP	=	5	DELTAY OR YUITE	=	0 .0442	SEP AT X	=	0 .371
ITERATION	130	CIR	=	0 .47060	DPM	=	0 .00007774	AT	2	10	NSSP	=	5	DELTAY OR YUITE	=	0 .0441	SEP AT X	=	0 .371
ITERATION	140	CIR	=	0 .47122	DPM	=	0 .00008567	AT	48	12	NSSP	=	5	DELTAY OR YUITE	=	0 .0440	SEP AT X	=	0 .371
ITERATION	150	CIR	=	0 .47188	DPM	=	0 .00007439	AT	46	7	NSSP	=	5	DELTAY OR YU TE	=	0 .0438	SEP AT X	=	0 .371
ITERATION	160	CIR	=	0 .47210	DPM	=	0 .00008565	AT	47	11	NSSP	=	5	DELTAY OR YUITE	=	0 .0438	SEP AT X	=	0 .371
ITERATION	170	CIR	=	0 .47255	DPM	=	0 .00005283	AT	45	2	NSSP	=	5	DELTAY OR YUITE	=	0 .0437	SEP AT X	=	0 .371
ITERATION	180	CIR	=	0 .47301	DPM	=	0 .00008582	AT	45	12	NSSP	=	5	DELTAY OR YUITE	=	0 .0436	SEP AT X	=	0 .371
ITERATION	190	CIR	=	0 .47347	DPM	=	0 .00021251	AT	48	13	NSSP	=	5	DELTAY OR YUITE	=	0 .0435	SEP AT X	=	0 .371
ITERATION	200	CIR	=	0 .47383	DPM	=	0 .00008394	AT	2	11	NSSP	=	5	DELTAY OR YUITE	=	0 .0434	SEP AT X	=	0 .371
ITERATION	210	CIR	=	0 .47438	DPM	=	0 .00018926	AT	48	12	NSSP	=	5	DELTAY OR YUITE	=	0 .0434	SEP AT X	=	0 .371
ITERATION	220	CIR	=	0 .47486	DPM	=	0 .00018582	AT	48	9	NSSP	=	5	DELTAY OR YUITE	=	0 .0433	SEP AT X	=	0 .371
ITERATION	230	CIR	=	0 .47531	DPM	=	0 .00007826	AT	2	10	NSSP	=	5	DELTAY OR YUITE	=	0 .0432	SEP AT X	=	0 .371
ITERATION	240	CIR	=	0 .47577	DPM	=	0 .00008886	AT	47	8	NSSP	=	5	DELTAY OR YUITE	=	0 .0432	SEP AT X	=	0 .371
ITERATION	250	CIR	=	0 .47622	DPM	=	0 .00009783	AT	48	13	NSSP	=	5	DELTAY OR YUITE	=	0 .0431	SEP AT X	=	0 .371
ITERATION	260	CIR	=	0 .47667	DPM	=	0 .00010988	AT	48	13	NSSP	=	5	DELTAY OR YUITE	=	0 .0431	SEP AT X	=	0 .371
ITERATION	270	CIR	=	0 .47712	DPM	=	0 .00010278	AT	48	13	NSSP	=	5	DELTAY OR YUITE	=	0 .0430	SEP AT X	=	0 .371
ITERATION	280	CIR	=	0 .47758	DPM	=	0 .00007882	AT	47	12	NSSP	=	5	DELTAY OR YUITE	=	0 .0430	SEP AT X	=	0 .371
ITERATION	290	CIR	=	0 .47800	DPM	=	0 .00008384	AT	47	8	NSSP	=	5	DELTAY OR YUITE	=	0 .0429	SEP AT X	=	0 .371
ITERATION	300	CIR	=	0 .47843	DPM	=	0 .00006717	AT	46	11	NSSP	=	5	DELTAY OR YUITE	=	0 .0428	SEP AT X	=	0 .371
ITERATION	310	CIR	=	0 .47885	DPM	=	0 .00012022	AT	47	9	NSSP	=	5	DELTAY OR YUITE	=	0 .0428	SEP AT X	=	0 .371
ITERATION	320	CIR	=	0 .47927	DPM	=	0 .00005227	AT	46	12	NSSP	=	5	DELTAY OR YUITE	=	0 .0428	SEP AT X	=	0 .371
ITERATION	330	CIR	=	0 .47968	DPM	=	0 .00018146	AT	3	11	NSSP	=	5	DELTAY OR YUITE	=	0 .0427	SEP AT X	=	0 .371
ITERATION	340	CIR	=	0 .48008	DPM	=	0 .00008214	AT	47	11	NSSP	=	5	DELTAY OR YUITE	=	0 .0427	SEP AT X	=	0 .371
ITERATION	350	CIR	=	0 .48047	DPM	=	0 .00012928	AT	48	6	NSSP	=	5	DELTAY OR YUITE	=	0 .0427	SEP AT X	=	0 .371
ITERATION	360	CIR	=	0 .48088	DPM	=	0 .00005338	AT	2	13	NSSP	=	5	DELTAY OR YUITE	=	0 .0426	SEP AT X	=	0 .371
ITERATION	370	CIR	=	0 .48124	DPM	=	0 .00005781	AT	2	11	NSSP	=	5	DELTAY OR YUITE	=	0 .0426	SEP AT X	=	0 .371
ITERATION	380	CIR	=	0 .48161	DPM	=	0 .00007863	AT	46	12	NSSP	=	5	DELTAY OR YUITE	=	0 .0426	SEP AT X	=	0 .371
ITERATION	390	CIR	=	0 .48198	DPM	=	0 .00012847	AT	48	11	NSSP	=	5	DELTAY OR YUITE	=	0 .0426	SEP AT X	=	0 .371
ITERATION	400	CIR	=	0 .48234	DPM	=	0 .00007378	AT	2	10	NSSP	=	5	DELTAY OR YUITE	=	0 .0426	SEP AT X	=	0 .371

BOUNDARY LAYER ANALYSIS FOR REYNOLDS NUMBER OF 0 .6000E+07

X	YUDRIC	DU	SLU	YLDRIC	DL	SLL
-0 .48000	0 .01706	0 .0	0 .81058	0 .01706	0 .0	0 .81058
-0 .48044	0 .03212	0 .00016	0 .38634	0 .03212	0 .00016	0 .38634
-0 .43087	0 .04070	0 .00021	0 .24376	0 .04070	0 .00013	0 .23974
-0 .40072	0 .04871	0 .00032	0 .17412	-0 .04871	0 .00015	0 .18847
-0 .37058	0 .05112	0 .00055	0 .13927	0 .05112	0 .00017	0 .13852
-0 .34028	0 .05438	0 .00058	0 .10138	-0 .05438	0 .00019	0 .09380
-0 .30982	0 .05877	0 .00111	0 .07221	0 .05877	0 .00022	0 .08868
-0 .27823	0 .05842	0 .00130	0 .04118	0 .05842	0 .00024	0 .04368
0 .24852	0 .05848	0 .00148	0 .03068	0 .05851	0 .00026	0 .03208
0 .21788	0 .05898	0 .00170	0 .01818	-0 .05898	0 .00028	0 .00683
0 .18877	0 .05898	0 .00182	0 .00113	-0 .05898	0 .00030	0 .00832
0 .15877	0 .05880	0 .00214	0 .01107	0 .05880	0 .00032	0 .01787

+0 13470	0 05805	0 00237	+0 03178	+0 00805	0 00036	0 03600
+0.003307	0.003776	0 00251	+0 03126	+0 00776	0 00036	0 03174
+0 03240	0 03843	0 00286	+0 03067	+0 00843	0 00036	0 04730
+0 03131	0 05488	0 00313	+0 04716	+0 05488	0 00040	0.06631
0.0	0 05304	0 00301	+0 05373	+0 05304	0 00043	0 06348
0 03131	0 05087	0 00371	+0 05952	+0 05087	0 00044	0 06088
0.003240	0 04888	0 00404	0 06481	+0 04880	0 00044	0 07488
0 03357	0 04618	0 00448	+0 06884	+0 04618	0 00048	0 08048
0 12470	0 04305	0 00479	+0 07348	+0 04305	0 00050	0 08556
0 18577	0 04060	0 00535	+0 07588	+0 04060	0 00052	0 09033
0 18577	0 03781	0 00578	+0 07848	+0 03781	0 00054	0 09482
0 21788	0 03490	0 00644	+0 07588	+0 03490	0 00058	0 09907
0.24852	0 03178	0 00728	+0 07237	+0 03178	0 00058	0 10315
0 27823	0 02858	0 00843	+0 06361	+0 02858	0 00058	0 10713
0 30582	0 02514	0 01018	+0 04283	+0 02514	0 00053	0 11084
0 34028	0 02188	0 01261	+0 01082	+0 02188	0 00070	0 11335
0 37088	0 01888	0 01684	0 00807	+0 01888	0 00051	0 11844
0.400772	0 01638	0 02106	0 02802	+0 01638	0 00057	0 11648
0 43867	0 01388	0 02527	0 05058	+0 01388	0 00115	0 12263
0 48044	0 00388	0 03256	0 08885	+0 00885	0 00135	0 12744
0 48000	0 00288	0 03615	0 14888	+0 00285	0 00183	0 13216

CP BY CENTRAL DIFFERENCES

X	CPU	CPL
+0 480	-2 888	1 082
+0 480	-2 473	0 803
+0 431	-2 438	0 606
+0 401	-2 482	0 482
+0 371	-1 782	0 372
+0 340	-1 882	0 303
+0 310	-1 382	0 251
+0 278	-1 231	0 208
+0 248	-1 104	0 175
+0 218	-0 987	0 148
+0 187	-0 881	0 127
+0 158	-0 814	0 108
+0 128	-0 736	0 088
+0 098	-0 661	0.088
+0 062	-0 593	0 078
+0 031	-0 528	0 088
0 0	-0 488	0 082
0 031	-0 418	0 088
0 062	-0 384	0 084
0 094	-0 288	0 082
0 126	-0 244	0 050
0 158	-0 158	0 048
0 187	-0 134	0 048
0 218	0 078	0 048
0 248	-0 018	0 048
0 278	0 068	0 052
0 310	0 108	0 058
0 340	0 133	0 051
0 371	0 128	0 068
0 401	0 158	0 071
0 431	0 178	0 078
0 460	0 188	0 075
0 488	0 217	0 162

X	VU	VL	SLL	SLL
+0 48000	0 01706	+0 01706	0 81058	+0 8 058
+0 48044	0 03227	+0 03229	0 [illegible]	0 [illegible]
+0 43867	0 04082	+0 04084	0 26336	[illegible]
+0 40072	0 04703	+0 04685	0 17412	+0 18947
+0 37088	0 05188	+0 05139	0 13827	+0 13882
+0 34028	0 05528	+0 05458	0 10138	+0 09280
+0 30582	0 05788	+0 05888	0 07231	+0 05588
+0 27823	0 05972	+0 05888	0 04918	+0 04184
+0 24852	0 06084	+0 05971	0 03058	+0 02606
+0 21788	0 06185	+0 06023	0 01815	+0 00883
+0 18577	0 06150	+0 06028	0 00112	0 00522
+0 18577	0 06174	+0 05932	+0 01107	0 01587
+0 12470	0 06122	+0 05820	+0 02178	0 02665
+0 06367	0 06040	+0 05815	+0 03128	0 03654
+0 03240	0 05928	+0 05881	+0 03867	0 04735
+0 03131	0 05783	+0 05530	+0 04716	0 05631
0 0	0 05638	+0 05338	+0 05373	0 05348
0 03131	0 04458	+0 05131	+0 05852	0 06081
0 03240	0 05285	0 04908	+0 06451	0 07498
0 03357	0 05058	+0 04884	+0 06884	0 08048
0 12470	0 04838	+0 04408	+0 07248	0 08554
0 18577	0 04607	+0 04132	+0 07588	0 09033
0 18577	0 04371	+0 03845	+0 07845	0 09482
0 21788	0 04135	+0 03545	+0 07810	0 09907
0 24852	0 03908	+0 03236	+0 07237	0 10315
0 27823	0 03685	+0 02911	+0 06361	0 10713
0 30582	0 03528	+0 02578	0 04283	0 11084
0 34028	0 03447	+0 02238	0 01082	0 11335
0 37088	0 03444	+0 01885	0 00807	0 11884
0 40072	0 03488	+0 01527	0 02802	0 11648
0 43867	0 03634	+0 01170	0 05058	0 12263
0 48044	0 03848	+0 00804	0 08885	0 12744
0 48000	0 04248	+0 00428	0 14888	0 13216

MACH CHART IN COMPUTATIONAL PLANE-FREE STREAM FROM TOP

I=2.46 TOP TO BOTTOM

J= 2.34 LEFT TO RIGHT

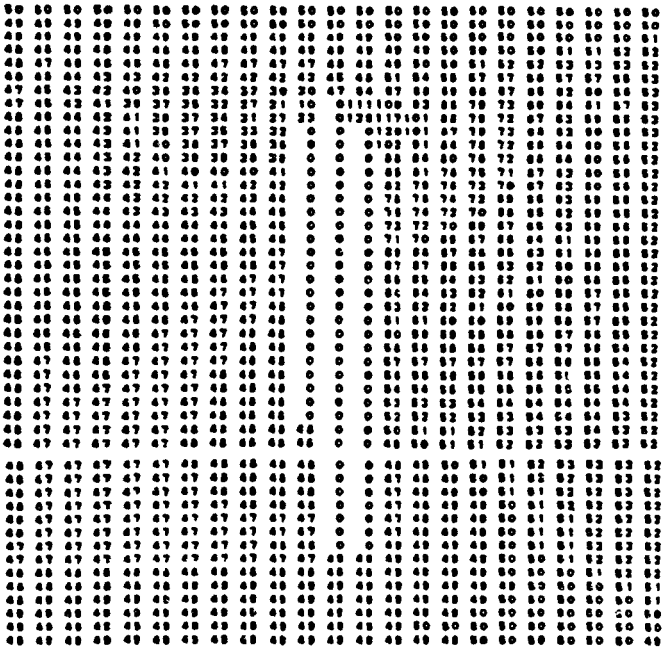

NORMAL FORCE COEFFICIENT CN BY INTEGRATION = 0.0202

WAVE CD = 0.003018
THEORETICALLY ZERO FOR SUBCRITICAL CASES

ORIGINAL PAGE IS
OF POOR QUALITY

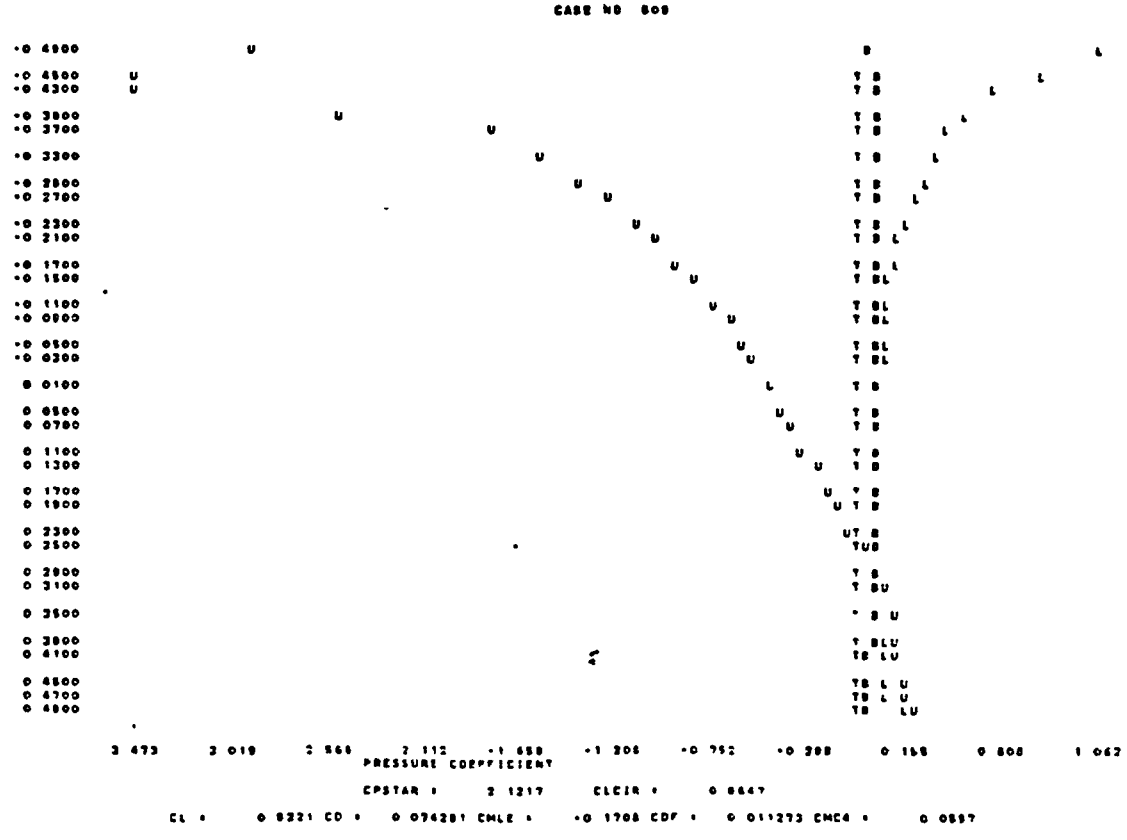

END

DATE

FILMED

JAN 22 1986

End of Document